R-09-40

Analysis of the effect of vibrations on the bentonite buffer in the canister hole

Martin Jonsson, ÅF – Berg och Mätteknik

Hossein Hakami, Thushan Ekneligoda,
Itasca Geomekanik AB

September 2009

Svensk Kärnbränslehantering AB
Swedish Nuclear Fuel
and Waste Management Co

Box 250, SE-101 24 Stockholm
Phone +46 8 459 84 00

ISSN 1402-3091
SKB Rapport R-09-40

Analysis of the effect of vibrations on the bentonite buffer in the canister hole

Martin Jonsson, ÅF – Berg och Mätteknik

Hossein Hakami, Thushan Ekneligoda,
Itasca Geomekanik AB

September 2009

Abstract

During the construction of a final repository for spent nuclear fuel in crystalline rock, blasting activities in certain deposition tunnels will occur at the same time as the deposition of canisters containing the waste is going on in another adjacent access tunnel. In fact, the deposition consists of several stages after the drilling of the deposition hole. The most vulnerable stage from a vibration point of view is when the bentonite buffer is placed in the deposition hole but the canister has not been placed yet. During this stage, a hollow column of bentonite blocks remains free to vibrate inside the deposition hole.

The goal of this study was to investigate the displacement of the bentonite blocks when exposed to the highest vibration level that can be expected during the drill and blast operations. In order to investigate this, a three dimensional model in 3DEC, capable of capturing the dynamic behaviour of the bentonite buffer was set up.

To define the vibration levels, which serve as input data for the 3DEC model, an extensive analysis of the recorded vibrations from the TASQ – tunnel was carried out. For this purpose, an upper expected vibration limit was defined. This was done outgoing from the fact that the planned charging for the construction of the geological repository will lie in the interval 2 to 4 kg. Furthermore, at the first stage for this study, it was decided that the vibration should be conservatively evaluated for 30 m distance. Using these data, it was concluded that the maximum vibration level that can be expected will be approximately 60 mm/s.

After simplifying the vibration signal, a sinusoidal wave with the amplitude 60 mm/s was applied at the bottom of the column and it was assumed that the vibrations only affect the bentonite buffer in one direction (horizontal direction). From this simulation, it was concluded that hardly any displacements occurred. However, when applying the same sinusoidal wave both in the horizontal and the vertical direction, the maximum deformation increased to approximately 22 mm in horizontal direction at the top of the bentonite buffer. On the other hand, when using a measured vibration signal in both vertical and horizontal direction with only one peak value (60 mm/s), it was concluded that the maximum displacements decreased rapidly. For this analysis, the maximum displacement was 0.35 mm for the uppermost bentonite ring. Thus, it can be concluded that when conducting blasting activities at 30 m distance with 4 kg of loading, the bentonite buffer will likely encounter a displacement which is less than 0.5 mm.

As no information could be obtained from the literature about the friction properties between the bentonite rings, a sensitivity analysis was carried out. From these results, it was concluded that the deformations primary depend on the applied vibrations and thus, the material properties might not affect the calculated deformations severely. Due to this reason, it is believed that no further investigation of the material properties has to be carried out for the current project.

Contents

1 Introduction

During the construction of a final repository for spent nuclear fuel in crystalline rock, blasting activities in certain deposition tunnels will occur at the same time as the deposition of canisters containing the waste is going on in another adjacent access tunnel. In fact, the deposition consists of several stages after the drilling of the deposition hole:

- Stage 1: Preparation of the deposition hole for deposition
- Stage 2: Placement of the bentonite buffer blocks
- Stage 3: Deposition of the canister containing the waste
- Stage 4: Backfilling and sealing of the deposition hole

Considerations about blasting in the vicinity of a sealed deposition hole have concluded that there should not be any risk for the functionality and safety of the deposition. Furthermore, the canister itself would not be affected by the blasting vibrations due to the much harder requirements on its design, material, strength and construction. On the other hand, it seems that the stage most vulnerable from a vibration point of view is; when the bentonite buffer is placed in the deposition hole but the canister has not been placed yet (Stage 2). In fact, in this condition, a hollow column of bentonite blocks of the height of 5.3 m remains free to vibrate inside the deposition hole as shown in Figure 1-1.

The evaluation of the risk for the integrity of the bentonite buffer requires the estimation of the entity and propagation of the vibrations induced by blasting and the effect of such vibrations on the buffer to determine the minimum safety distance between the location of the blasting and the deposition hole. The main risk is that the blasting induced vibrations produce sliding of the bentonite blocks with respect to each other. This could lead to a radiation hazard in case the canister would get stuck between the bentonite blocks during deposition.

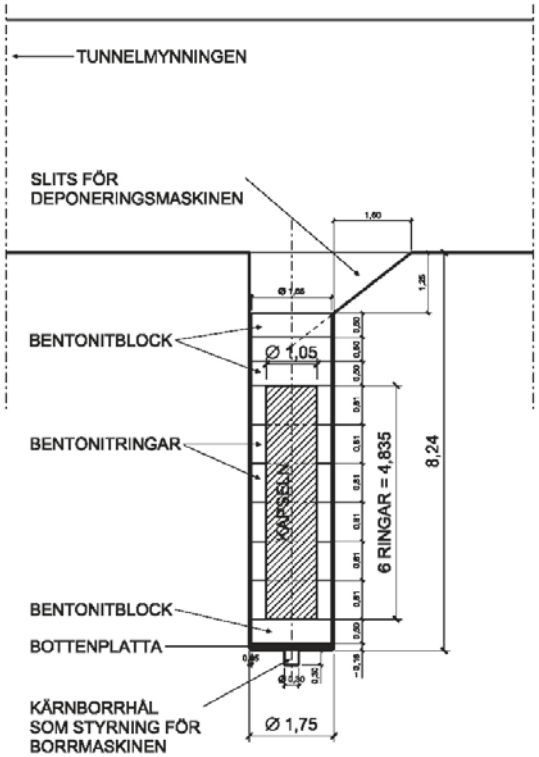

Figure 1-1. *Geometry of the deposition hole, bentonite buffer and canister containing the waste. The gap between the rock and the bentonite blocks is 5 cm.*

From a design point of view, the distance between two deposition tunnels is determined based on: i) the thermal properties of the rock mass; ii) the amount of heat the spent nuclear waste can produce; iii) the maximum temperature allowed at the interface between the canister and the buffer and between the buffer and the rock and; iv) other consideration about optimization of the economy of the construction of the repository facility. These considerations have led to a minimum distance between the deposition tunnels of 40 m.

A preliminary evaluation indicates that a distance between the blasting and the deposition hole shorter than 80 m could jeopardize the integrity of the buffer. To guarantee that the level of vibration after the positioning of the buffer is not too high, it has therefore been assumed that the blasting cannot take place closer than two deposition tunnels away from the placed buffer.

1.1 Objectives

The case with vibrations on the installed buffer blocks during the deposition is considered the most critical and will be extensively studied in this report. It is expected that in this configuration the vibrations can cause sliding of the block with problems during canister deposition due to geometrical tolerances or even mechanical damage of the ring-shaped blocks. The goal of this study is therefore to investigate the deformations of the bentonite buffer when exposed to the highest vibration level than can be expected when blasting is performed. For this purpose, a model that predicts the propagation of the vibrations in a rock mass with existing tunnels will be set up based on vibration data presented in /Nyberg et al. 2005/.

1.2 Outline of the report

In order to give the reader an overview of the geological conditions at the area of interest, a brief summery is presented in Chapter 2. As no blasting experiments were carried out within this project, already collected data were reanalysed (from the TASQ – and TASS tunnels). To calculate the deformations in the bentonite buffer when exposed to blast induced vibrations, the vibration signal must be characterised. This analysis and the corresponding assumptions are presented in Chapter 3. Thereafter, in Chapter 4, the necessary input data to model the friction behaviour between the bentonite rings are given. In Chapter 5, the 3DEC model developed within this project is presented together with the results and the carried out sensitivity analysis.

2 Site description

During the first half of 2003, a 70 m long tunnel named APSE (Äspö Pillar Stability Experiment) was blasted in hard crystalline rock at the Äspö HRL (Hard Rock Laboratory) in Sweden /Andersson 2003/. The dominating rock types in the Äspö area are the plutonic Äspö diorite and Ävrö granite. They belong to the postorogenic phase of the Transscandinavian Igneous Belt (TIB); their ages are c 1.8 Ga. The Äspö diorite is a medium-grained, grey to reddish grey rock. It is generally porphyritic, with K-feldspar megacrysts.

The TASQ tunnel is dominated by different varieties of Äspö diorite (see Figure 3-2 for the location of the TASQ – tunnel). The "Äspö diorite" is a quarz-monzodiorite. The major rock volume consists of unaltered Äspö diorite, but relatively large volumes also consist of oxidized or sheared Äspö diorite. This is primarily associated with a ductile deformation zone that strikes in the tunnel orientation and dips approximately 45 degrees to SE. Other rock types present are mafic rocks, pegmatite and fine-grained granite. Rock contacts are generally diffuse, as they are successive transitions from one type of Äspö diorite to another. Contacts between dikes and host rock are sharp, but well healed. Regional metamorphism appears to be absent or of very low grade in the TASQ rock volume. Occasionally a diffuse foliation can be found in the Äspö diorite, which appears to be associated with the regional foliation pattern. Hydrothermal, low grade alteration appears to some extent in association with the old ductile deformation zone that strikes along the tunnel.

3 Vibration analysis

The vibrations induced by the blasting in the TASQ Tunnel were recorded by geophones placed in several surrounding tunnels and analysed and presented in /Nyberg et al. 2005/. In the present report, these data were used to predict the peak particle velocity that the bentonite buffer can be exposed to.

This chapter summarizes the vibration measurements performed in the TASQ tunnel, and presents the extended analysis carried out to characterise the vibration signal to be used for the numerical simulations of the dynamic behaviour of the bentonite rings given in Chapter 5.

3.1 Description of performed vibration measurments

During the blasting operations, the vibrations were measured using geophones and the Ava95 system, which is a software system supplied by Bergsäker AB and used to record the vibrations, see Figure 3-1.

The geophone network used to record the vibrations can be seen in Figure 3-2. All geophones measured the vibrations in vertical direction except geophone PA3514B01, which measured the vibration in three orthogonal directions. In /Nyberg et al. 2005/, the geophones were tuned so that frequencies over 350 Hz were filtered out.

The measured vibration level depends on the direction between the blasting point and the point where the vibrations are measured. The reason is that a vibration, in general, consists of two different types of waves, P-wave (primary) and S-wave (shear). These two types of waves propagate with different speeds through the rock mass. The first wave that reaches the geophone will be the P-wave. This implies that for a blasting that occurs next to a tunnel, the largest vibration will be measured perpendicular to the tunnel wall and not necessarily in the vertical direction. This is the case for a blasting done

Figure 3-1. *Recording unit Ava95 and geophones for vibration measurement.*

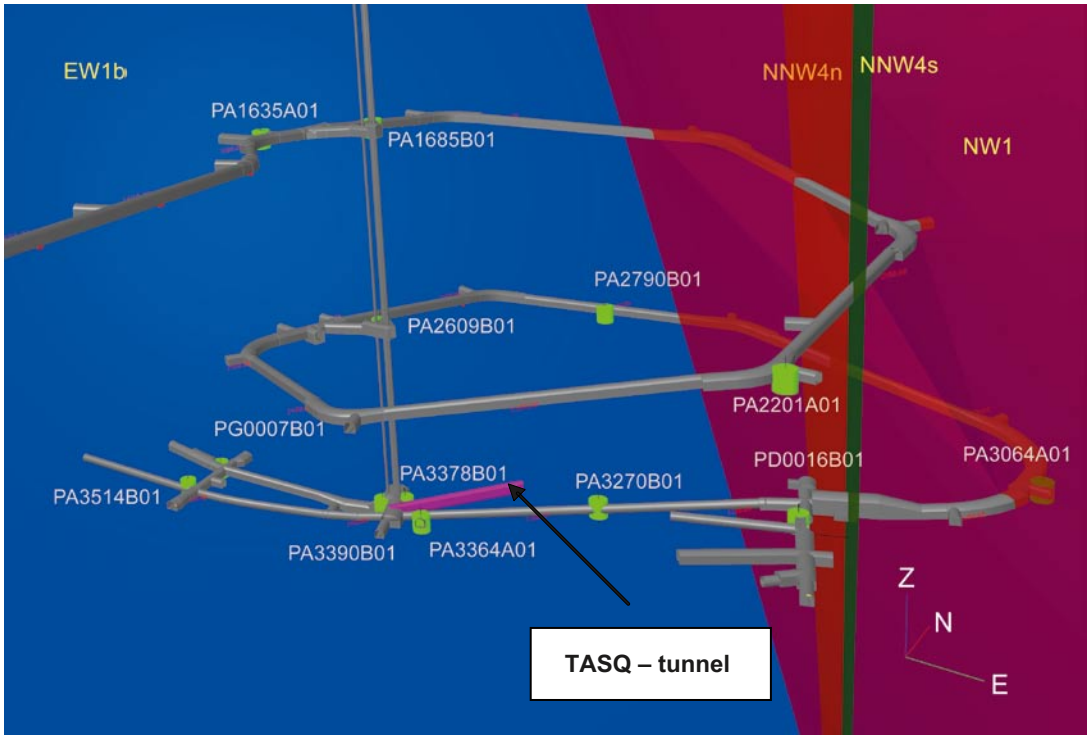

Figure 3-2. *Picture showing the geophone network used to record the vibrations, which are studied in this study. Picture reproduced after /Nyberg et al. 2005/*

above a tunnel, where the maximum vibration will be measured in vertical direction. This fact can be observed when studying the data points given in /Nyberg et al. 2005/ where the vertical direction always gives the lowest vibration for the three-directional geophone PA3514B0. However, in this report no consideration was taken to the fact that the amplitude depends on the direction along which the vibrations were measured.

3.2 Evaluation of the vibration signal to be used in the numerical models

In this section, the vibration signal that will be used for the numerical simulations of the dynamic behaviour of the bentonite rings, which is presented in Chapter 5 are defined. When characterising the vibration level, both the amplitude and the frequency are needed as indicated below

$$v = A\sin(f\,2\pi t) \qquad 3\text{-}1$$

where A is the amplitude, f the frequency and t the time. Thus, the input data needed for the numerical modelling are the maximum expected vibration amplitude and the upper and lower frequency that can be expected in the vibration signals. The reason why a lower frequency limit also has to be defined is that resonance effects can occur with a higher probability for low frequencies. Furthermore, in order to fully define the vibration signal, the duration of the acting vibration on the construction must be given.

3.2.1 Evaluation of the maximum vibration amplitude

In order to predict the peak particle velocity as a function of the distance between the point of detonation and the point of interest, a commonly used method is to use a scaling law as indicated below

$$PPV = K \cdot \left(\frac{R}{\sqrt{Q}} \right)^{n} \qquad 3\text{-}2$$

where R is the distance between the detonation and the point of interest, Q is the charging weight and PPV is the peak particle velocity. The two coefficients n and K have specific values depending upon the rock mass properties between the location of the blasting and the measurement point. These coefficients primarily depend on factors like the type of wave that is propagating in the rock, the geology, etc. In Figure 3-3, the peak particle vibration level as function of scaled distance for the five different datasets evaluated in /Nyberg et al. 2005/ (five solids lines) are plotted. Each of them shows how PPV decreases with the scaled distance, which is defined as the distance divided by the square root of the charge used for the particular blast round. The coefficients n and K used for plotting the attenuation lines in Figure 3-3 are given in Table 3-1.

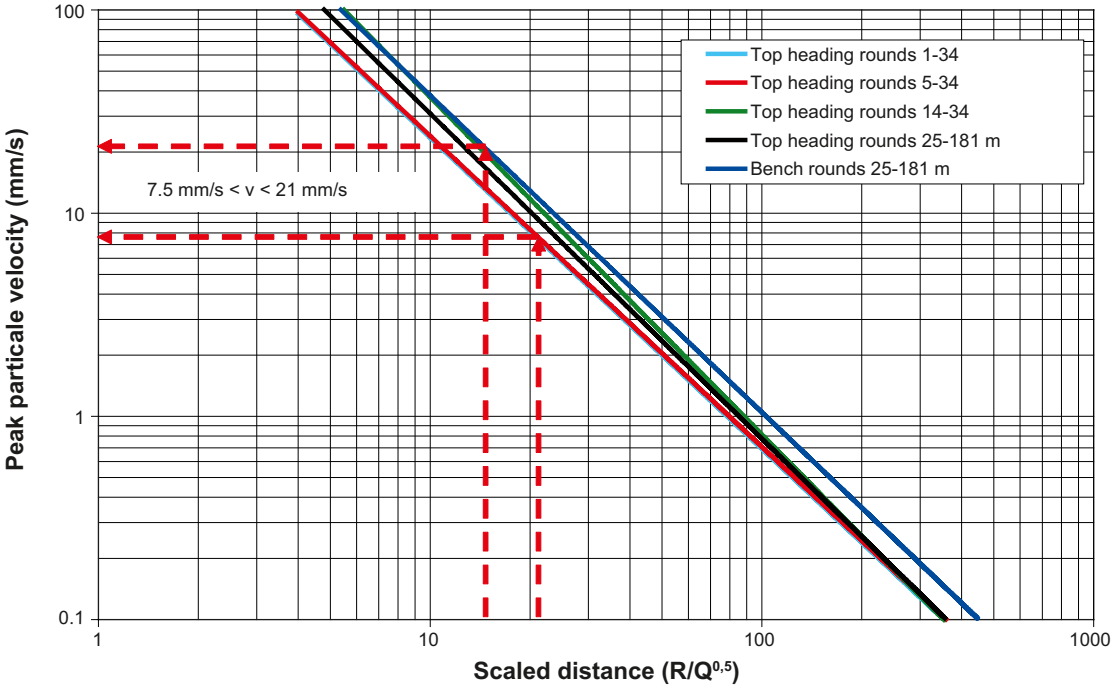

Figure 3-3. *Peak particle vibration level as function of scaled distance for five different dataset evaluated in /Nyberg et al. 2005/. The solid lines shown are fitted using the least square method and the underlying data points are not shown.*

Table 3-1. Fitting parameters for log PPV data with 95% prediction confidence limits for intercept line with parameters A and slope n. Data reproduced after /Nyberg et al. 2005/.

Data set	Parameters	Mean
Top heading Rounds 1–34	Log K	2.90
419 values	n	–1.53
Top heading Rounds 5–34	Log K	2.91
370 values[1]	n	–1.53
Top heading Rounds 14–34	Log K	3.23
299 values[2]	n	–1.66
Top heading 25–181 m	Log K	3.09
192 values	n	–1.60
Bench 25–181 m	Log K	3.14
58 values	n	–1.56

1 Test rounds and misfired rounds are excluded.

2 Full blast rounds with 100–138 blast holes.

According to Rolf Christiansson (personal communication 13/06/2008), the planned charging for the construction of the geological repository will lie in the interval 2 to 4 kg. Furthermore, as indicated in /Lindman et al. 2007/, the blasting will take place 80 m meters away from the bentonite buffer. However, at the first stage for this study the vibration shall, according to project specifications be conservatively evaluated for 30 m. When using these two input values, the average expected level of vibration can be calculated and ranges approximately from 7.5 mm/s to 21 mm/s (Figure 3-3). On the other hand, it can be seen that when assuming the blasting to occur at 80 meters distance, the expected range will be 2 mm/s to 5 mm/s. Thus, a rapid decrease in *PPV* as a function of increasing distance is obtained.

As seen in Figure 3-3, the datasets differ. When investigating the underlying data points in more detail, a large scatter can be found (Figure 3-4). There might be several reasons for this: one is that the vibrations are measured mostly in one direction, in this case vertical direction as explained in Section 3.1. Other causes can be that the charge in one blast hole has initiated simultaneously as another hole and thus causing the simultaneous charge to increase, which leads to larger vibration. Finally, the natural scatter should be considered.

In order to make sure that the predicted level of vibration will not be exceeded, a statistical analysis of the prediction interval was carried out based on the original data presented in /Nyberg et al. 2005/. For this purpose, the 95% prediction interval was used. When using the expected charging weight of about 2 to 4 kg, it can be seen that the *PPV* will be in the interval between 30 and 55 mm/s when the distance is about 30 m and the upper 95% line is used. In other words, the probability that the peak particle velocity will be below 55 mm/s is 95%.

No underlying data points were analysed for the bench rounds, which give the highest vibration level (Figure 3-3). Only the top heading rounds 1 to 34 were used for this analysis. The reason for selecting this dataset was that it contains most data and therefore has the largest statistical base. In order to account for the higher vibration caused by bench blasting, a comparison of all the *K*-values (Table 3-1) for the scaling law obtained by the least square fit was carried out. As it can be seen in Table 3-1, the *K*-value is approximately 8.3% higher for the bench than for the top headings rounds 1 to 34. To take into account this fact, the maximum vibration level was increased by approximately 10% (even though this is not a completely scientific approach). Thus, *PPV* is estimated to 60 mm/s when performing the blasting with 4 kg and 30 m away from the bentonite buffer.

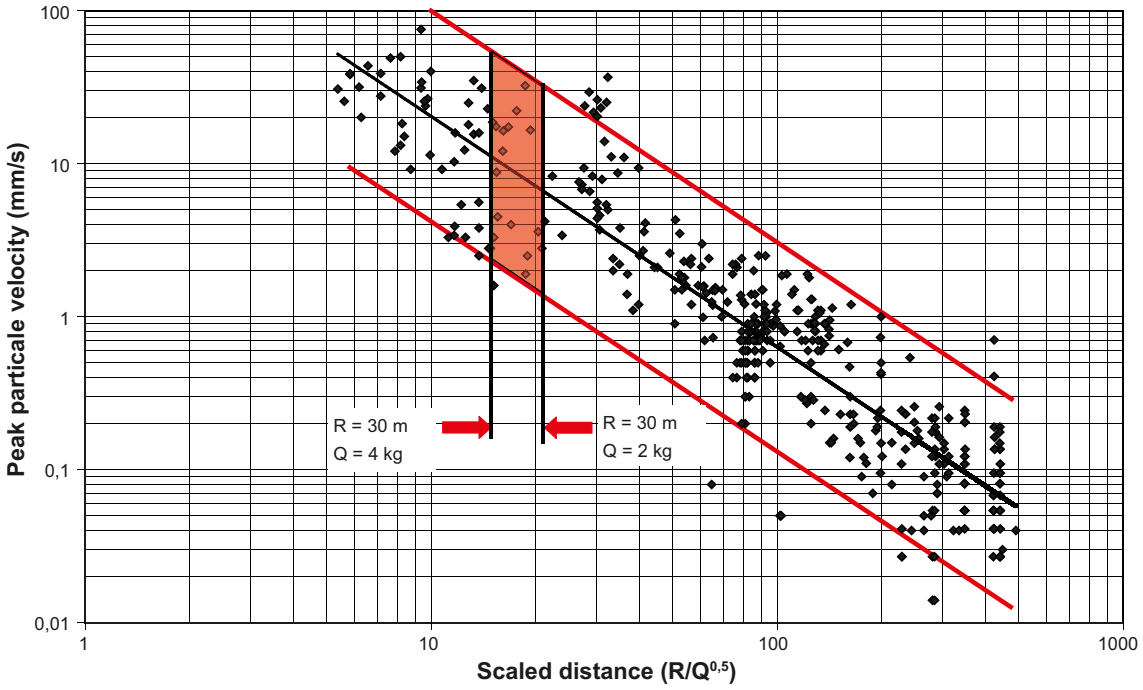

Figure 3-4. *Peak particle vibration level as a function of scaled distance. The solid black line indicate the least square fit and the red lines, the upper and lower 95% prediction interval. The original data are published in /Nyberg et al. 2005/ and used when evaluating the vibration for the top heading rounds 1 to 34.*

3.2.2 Evaluation of the upper and lower frequency of the vibration signal

When characterising the vibration signal, both the amplitude and the frequency must be defined as shown in Equation. The purpose of this section is to define the upper and lower frequency that can be expected to occur during the vibration.

The dominating frequency of a blast induced vibration is difficult to assess as it depends on the distance from the source, the material properties of the rock and possible fracture and deformation zones in the rock mass. As indicated by /Bodare 1997/, the damping of the vibration level depend on the dominating frequency: for high frequencies, a larger damping can be expected than for low frequencies. A consequence of this is that the dominating frequency will be lower when the blasting is performed at a long distance from the measuring point. A large range of the dominant frequencies measured during blasting experiments is given in the literature. For example, /Fredriksson et al. 2004/ mention the range 100–350 Hz whereas /Wersäll 2008/ mention that this range should be between 200 and 500 Hz. Thus, a large variation can be expected in the dominant frequency.

To obtain realistic values for the frequency to be expected in the ÄSPÖ region, blasting vibrations from the most recent blasting rounds (i.e. the TASS – tunnel) were evaluated. This analysis gave that the average dominant frequency is approximately 315 Hz for the seven rounds included in the analysis (Table 3-2). The dominant frequency in this case is evaluated for the vibrations caused when blasting the wedge.

When investigating a recorded vibration signal, the dominant frequency can be difficult to detect without further analysis. A common tool to determine the dominant frequency is to perform a frequency analysis by means of a Fast Fourier Transformation (FFT). Due to the large variation of the dominant frequency as indicated by /Fredriksson et al. 2004/ and /Wersäll 2008/, and from the evaluation of the experiments in the TASS tunnel (Personal communication with Rickard Karlzen 2008-07-11), it was decided to define the upper frequency limit of the vibration signal for this project to be 300 Hz. This value also corresponds to the maximum frequency that is specified in Swedish Standard /Svensk Standard SS 460 48 66 1991/, where it says that frequencies over 300 Hz shall be filtered out. However – and strictly speaking this standard is valid only for vibrations measurements on buildings on the ground surface.

For the definition of the lower frequency limit, resonance effects must be considered. This happen when the natural frequency of the pile of bentonite blocks matches the dominant frequency of the vibration. As shown in Figure 3-5, the dynamic magnification due to resonance depends on the damping factor and the ratio between the frequency of the applied load f_a and the frequency of the system itself f_s.

In order to calculate the natural frequency of the pile of bentonite blocks, simplifications must be made as the pile of bentonite is a complex mechanical system with distributed mass and stiffness and hence has a Multi-Degrees-Of-Freedom (MDOF) system. If assuming the pile of bentonite blocks to be solid (i.e. that the ring-shaped blocks are glued together), the first natural frequency of the system

Table 3-2. Dominant frequency evaluated for the vibrations caused when blasting the wedge for the TASS – tunnel.

Blast round (Nr)	6	7	8	9	10	11	12
Frequency (Hz)	300	278	400	354	265	297	307

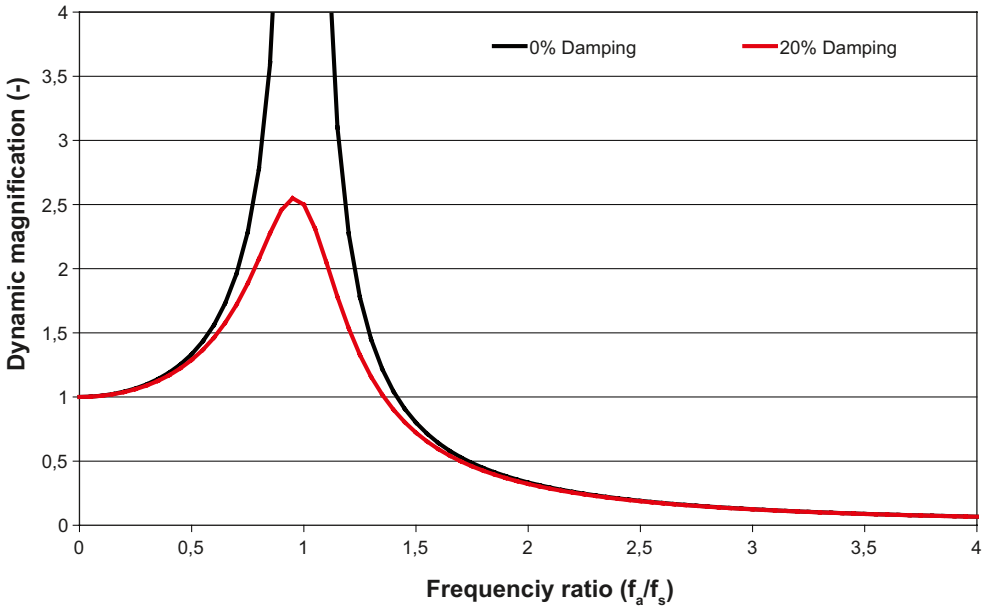

Figure 3-5. *Dynamic magnification factor for different damping rations as function of the ratio between the frequency of the applied load and the frequency of the system itself.*

can be calculated if the boundary conditions are known. However, for the investigated system, the boundary conditions are difficult to be assessed as slipping can occur between the lowest ring and the underlying copper plate as well as between the blocks. When assuming fixed boundaries, as rotation hardly can occur between the cupper plate and the lowest solid block, the analytical expression for f_1 is given in /Bachmann and Ammann 1987/:

$$f_1 = \frac{1}{2\pi}\sqrt{\frac{k^*}{m*}} \text{ with } k^* = \frac{3EI}{L^3} \text{ and } m^* = m_t + 0.23u_b \qquad 3\text{-}3$$

where E is the Young's modulus, I is the bending moment of inertia, L is the length of the cantilever beam, k is the bending stiffness of the beam, m_t is the concentrated mass at the beam tip and u_b is the distributed mass per meter. In order to calculate f_1, the following properties where used:

$L = 5.335$ m

$E = 321.7$ MPa

$\rho = 2{,}090$ kg/m^3

$A = \frac{\pi}{4}(1.63^2 - 1.07^2) = 1.1875$ m^2

$I = \frac{\pi}{64}(1.63^4 - 1.07^4) = 0.2822$ m^4

$u_b = 2{,}493 \frac{\text{kg}}{\text{m}}$

For the above values, f_1 can be estimated to be 8.9 Hz. However, no consideration was given to the fact that the lowest block is a solid disk and not ring-shaped. If we consider that the fixed boundary condition is too stiff to capture the "true" dynamic behaviour of the system (some sliding between the lowest plate and the cupper can be expected), the conclusion must be that f_1 should be lower than approximately 9 Hz as a softer boundary will decrease the natural frequency.

Blast induced vibrations tend to have much larger frequencies than 9 Hz, as indicated by /Fredriksson et al. 2004/ and /Wersäll 2008/. Therefore, it is not realistic to use a value much lower than 9 Hz when characterising the load to be applied to the numerical modelling of the system. In order to investigate the effect of the applied load, the value of 9 Hz was chosen as the lowest frequency limit.

3.2.3 Evaluation of the duration of the vibration

It is important to define the duration or maximum time during which the vibration will take place. In fact, a dynamic system can have its maximum response after the vibrations have damped out. According to the vibration measurements carried out earlier in the TASQ Tunnel and presented in /Nyberg et al. 2005/, the vibration signal lasts approximately 7 to 8 seconds. In this study, the duration of the blasting signal is set to 7 seconds. Due to practical reasons, the duration was chosen toward the lower range because the numerical simulation time will decrease by about 12% when going from 8 to 7 seconds.

3.3 Discussion and uncertainties when characterising the vibration signal

In order to estimate the maximum vibration level that the bentonite buffer can be exposed to during the drill and blast operations in the access tunnels, the following assumptions were made:

- The geological conditions affect the vibration level. For this study, it was assumed that the same geological conditions can be expected around the TASQ tunnel as for the final repository.
- The level of vibration will be affected by the frequency filter used in the measurement devices. According to the Swedish Standard /Svensk Standard SS 460 48 66 1991/, the vibrations shall be measured using a low-pass filter between at least 5 and 300 Hz. However, for the vibrations used to evaluate the maximum amplitude in this study, frequencies between 5 and 350 Hz were used.
- As indicated by /Fredriksson et al. 2004/ and /Wersäll 2008/, the frequency content can be expected to be in the interval between 100 and 500 Hz, which indicate a large variation. Due to this large expected variation, it is difficult to suggest one single value of the frequency and therefore the average value of 300 Hz was selected here. This value is also close to what was found when analysing the vibration signals from the TASS tunnel as indicated in Table 3-2.
- Furthermore, due to the above mentioned uncertainties and the fact that the frequency content of the signal only can be estimated or measured during the actual blasting activities there are large uncertainties in the determination of both the maximum amplitude and the frequency span to which the numerical model of the system should be loaded.

4 Evaluation of the friction angle between the bentonite blocks

4.1 Introduction

As no measurements of the frictional coefficient between two blocks of bentonite could be found in literature, Clay Technology AB performed a laboratory experiment in order to roughly quantify its value. This section presented the performed experiments, the experimental results and gives a short discussion on the reliability of the obtained data.

The maximum frictional force between two surfaces is proportional to the normal load acting on the surfaces where the proportionality constant is the frictional coefficient μ. The frictional coefficient is equal to the tangent function of the friction angle. The maximum frictional force is experienced just before the two surfaces start to slide with respect to each other.

4.2 Laboratory set-up

To estimate the frictional coefficient between two blocks of bentonite, a small block of compacted bentonite is placed onto another larger block of the same material.

The water content of the blocks was about 10% and their density of about 2,100 kg/m^3. The surfaces of the blocks in contact were even except for the striations obtained by saw-cutting the blocks.

The small black was tied by a rope with a force-meter. By dragging the rope parallel to the contact surface between the blocks, the frictional force was observed to increase until the small block started to glide. The maximum frictional force was recorded for different contact normal loads, starting by the self-weight of the smaller block (288.04 g) up to about 2 kg that were applied on top of the small block. Pulling of the smaller block was done parallel to the striations of the contact surface so that these would not affect the results.

4.3 Experimental results

The measured values of the forces and the frictional coefficients determined in the experiments are shown in Figure 4-1. The calculated frictional coefficient was in average 0.371 that corresponds to an average friction angle of 20.4°.

4.4 Discussion

The relation between the normal and frictional forces obtained in the experiment appears to be rather linear, which confirms that the test and measurements were made correctly. However, accuracy of the performed measurements was not investigated which means that the reported values apply only for blocks of similar size, water content, density and for saw-cut contact surfaces.

Furthermore, as this investigation was initiated due to lack of data and performed under time pressure, the presented data must be consider being rough and used by caution.

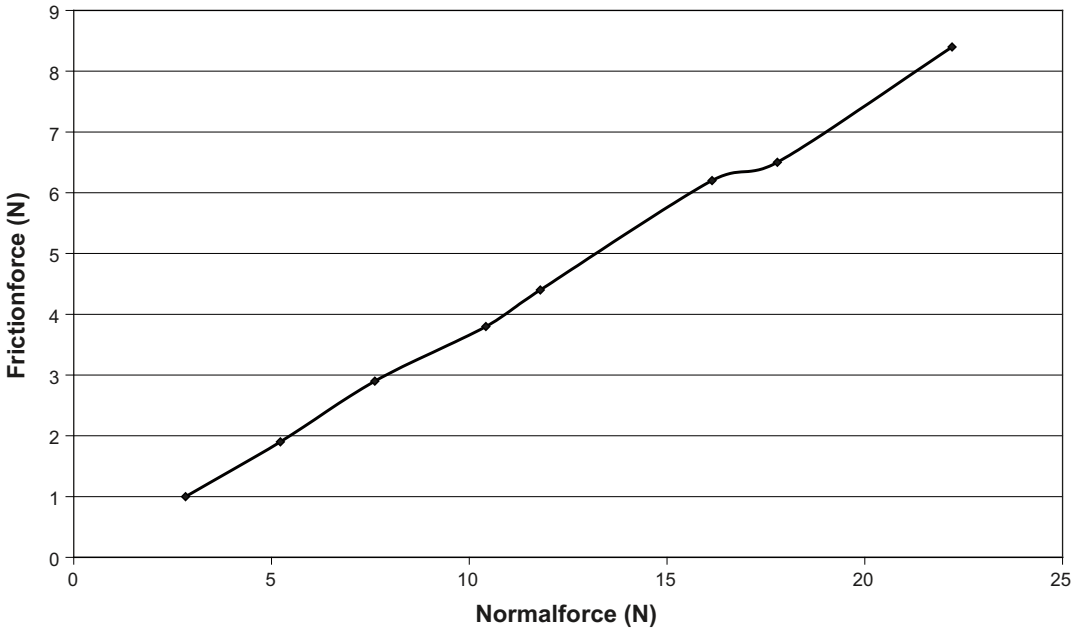

Figure 4-1. *Measured forces and calculated frictional coefficient and friction angle for two bentonite surfaces obtained by saw-cutting.*

5 3DEC model of the bentonite barrier

The main objective with this project was to investigate the behaviour of the bentonite barrier when exposed to blast induced vibrations. As hardly any deformations can be expected within the bentonite rings, it was decided to use the three dimensional discrete element code 3DEC. 3DEC is a numerical program based upon distinct element method /Itasca 2008/ that models the behaviour of discontinuum environments. In essence, it is a dynamic code that can simulate events like blasting, earthquake etc.

Figure 5-1 shows the geometry of the numerical model created within 3DEC, which consists of a levelling pad made of concrete (A), a disc (B) and six rings (C) made of bentonite clay. The levelling pad stands on a copper plate (yellow), interfacing the levelling pad (red) and the overlying bentonite ring (C). The disc (B) and rings (C) were modelled with approximated circles in which case the surface area of the contact planes of the approximated rings have 96% of the real rings. The change in natural frequency of the real bentonite structure and the approximated bentonite structure is estimated to be lower than 2.5% which is considered to be negligible. The dimensions of the different elements and their mechanical properties are given in Table 5-1. The mechanical properties for the interface between the bentonite rings such as the friction angle and the cohesion were provided by Clay Technology (2008) and reported in Chapter 4.

Free boundary conditions were maintained for the surfaces of the bentonite barrier as the disc (B) and rings (C) are free to move in any direction without any constraints. Figure 5-2 shows sections from the bentonite barrier.

Contact planes between the components of the bentonite barrier were modelled as stiff joints following a Mohr-Coulomb behaviour – thus the maximum shear force $F^s_{\max}$ in the contact planes can be derived according to equation as given in /Itasca 2008/

$$F^s_{\max} = cA_c + F_n \tan\phi \qquad 5\text{-}1$$

where c and φ are the joint cohesion and friction angle meanwhile A_c and F_n describe the contact area and the vertical load, respectively. The properties of the contact planes are given in Table 5-2.

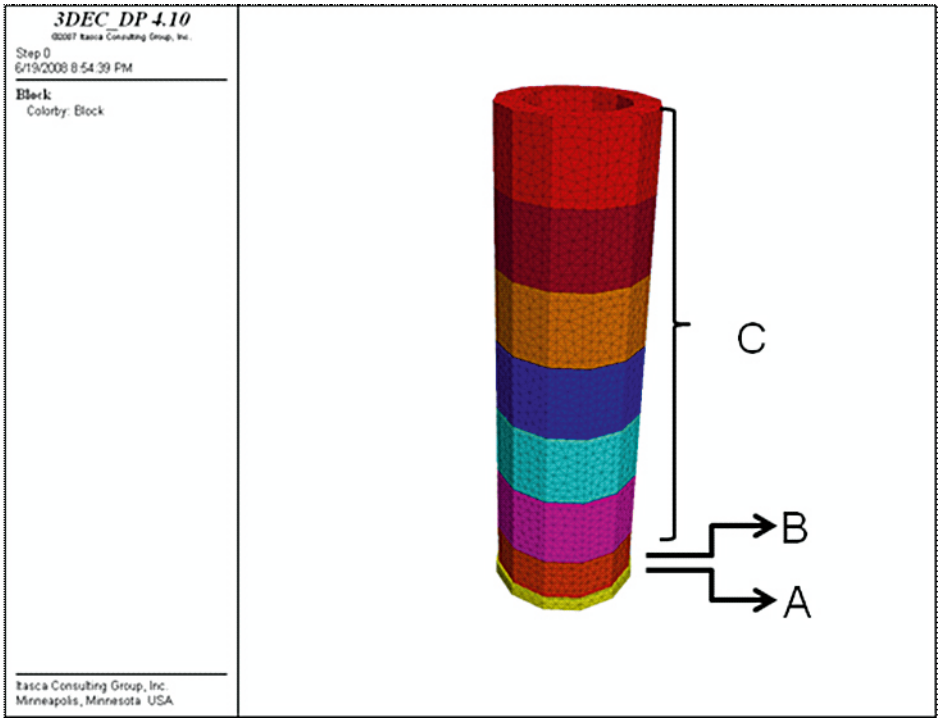

Figure 5-1. *Schematic figure that shows the elements included in the model – the levelling pad made of concrete (A), a disc (B) and six rings (C) made of bentonite clay.*

Table 5-1. Mechanical properties and geometrical properties of levelling pad and bentonite rings.

Type	Geometrical properties	Mechanical properties
Levelling Pad	Height 0.16 m	Density 2,650 kg/m^3
	Diameter 1.70 m	Shear modules 10.00 GPa
		Bulk modules 16.67 GPa
Solid bentonite ring	Height 0.5 m	Density 2,070 kg/m^3
	Diameter 1.63 m	Shear Modules 0.133 GPa
		Bulk Modules 0.185 GPa
Hollow bentonite rings	Height 0.80 m	Density 2,070 kg/m^3
	Outer diameter 1.63 m	Shear Modules 0.133 GPa
	Inner diameter 1.07 m	Bulk Modules 0.185 GPa

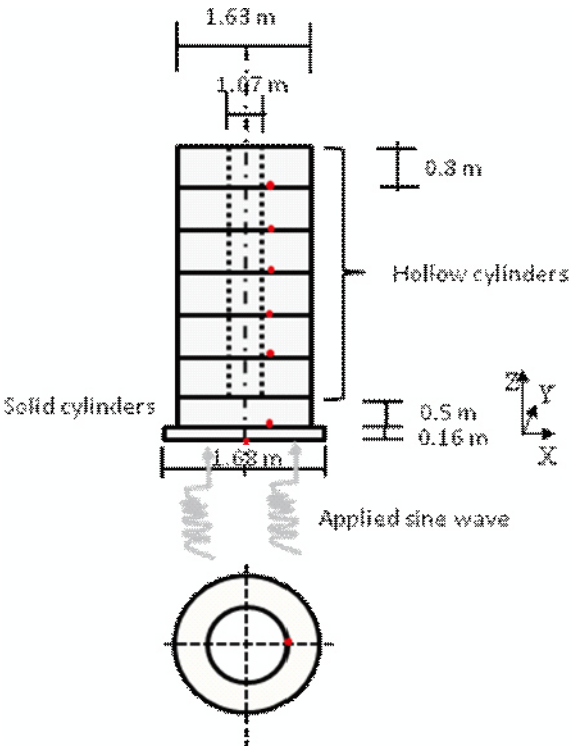

Figure 5-2. *3DEC model of the wave propagation in bentonite rings.*

Table 5-2. Mechanical properties of the joints.

Properties	Value
k_n (GPa/m)	10.0
k_s (GPa/m)	0.50
Cohesion (MPa)	0.0
Friction angle (°)	15°
Tensile strength (MPa)	0.0

While the column was completely free from any constrains and loaded by its own weight (gravity), it was exposed to a vibration through a sinusoidal wave form applied at the bottom of the column with specifications given in Table 5-3. As no specific data about the impulse load was available, at the phase one of the study, it was decided to use the simple form of impulse load (sinusoidal wave) which then simulates a conservative case. However in the phase two of the study the real shape of the dynamic signal is taken into account. A simulation run included the following stages:

1. The model was brought to equilibrium under gravitational load.
2. The sinusoidal wave form, as specified, was applied to the bottom of the model and the excitation lasted for 7 seconds.

5.1 Effect of blast vibration on the bentonite barrier

To investigate the effect of vibration induced by the nearby blasting, several cases were analyzed. These were:

1. The wave propagation was assumed to have only a horizontal component coinciding with the x-axis in a plane at right angle to the vertical axis of the column (For the x-, y- and z-direction please see Figure 5-2).
2. The wave propagation was assumed to occur in the horizontal plane for both the x- and y-axis components.
3. The effect of wave propagation in the vertical plane was analyzed using a horizontal plane wave in the X-direction and a vertical plane wave in the Z-direction.

Furthermore, a number of sensitivity analyses were performed in which the mechanical properties of the elements in the column and the vibration specifications were varied.

The first analysis, entitled as the “base case” includes the following parameters and is based on the analysis in Chapter 3 where the vibrations signal was characterised. For this analysis, the wave was assumed to be sinusoidal with the following properties (f = 300 Hz, wave length = 20 m, amplitude = 0.06 m). The joint properties for the cohesion and the friction angle were 0 MPa and 15°. The behaviour of the model was investigated at every history points in Figure 5-3. At history point 1 the velocity and displacement were monitored whereas in all the other points only the displacement was monitored. In the second phase of the study a measured vibration signal was used as the dynamic input in order to quantify how conservative the approach with a sinusidal signal is.

Table 5-3. Properties of the input wave for the numerical model.

Properties	Value
Frequency (Hz)	300
Velocity (m/s)	6,000
Exposure Time (s)	7

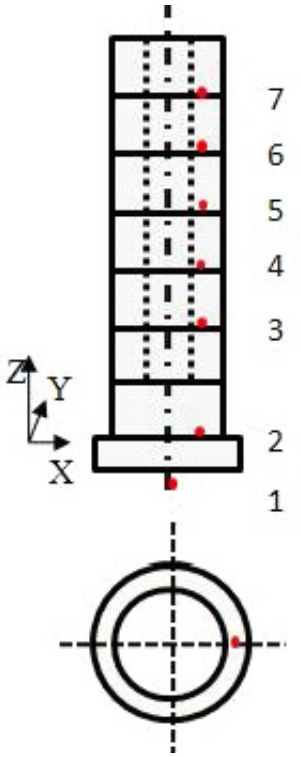

Figure 5-3. *Locations of history points used to investigate the deformations in the model.*

5.2 Wave propagation analysis

5.2.1 Wave propagation in X-direction

Figure 5-4 shows the variation of the particle velocity along the x-axis (for the last part of the vibration signal) for the base case at the history point 1 which verifies that the boundary condition is properly applied at the bottom of the levelling pad. In Figure 5-4 the variation of X-displacement against time is shown. Likewise the particle velocity, the displacement of history point 1 follows the sinusoidal wave form.

The displacement of the contact planes monitored at history points 2–7 (see Figure 5-3) follows an identical behaviour as in Figure 5-6, which shows the displacement for history point 3. The results for other history points are given in Appendix 1.

The maximum displacements when applying the load in the X-direction are summarized in Table 5-4. The largest displacement occurs at history point 7 and is 1.60 mm. The location of the largest displacement (point 7) may be explained by combining the attenuation of the wave and the friction mobilized across the contact planes before slip takes place. As the frequency of the wave is noticeably high, attenuation of the wave takes place rapidly when it travels upwards in the column. In contrast, the frictional resistance is mobilized, being a function of the normal load (weight of the column) and diminishes gradually higher up in the column.

5.2.2 Wave propagation in X- and Y-directions

In this stage, the base case wave is complemented with a Y directional wave applied at the base of the column. Both waves have the same wave properties and a zero phase angle was assumed between the two directions, which probably is a conservative assumption. The history points used were the same as for the base case, which is shown in Figure 5-3. In Figure 5-7, the X and the Y-displacement for history point 3 can be seen. The results for other points are presented in Appendix 2.

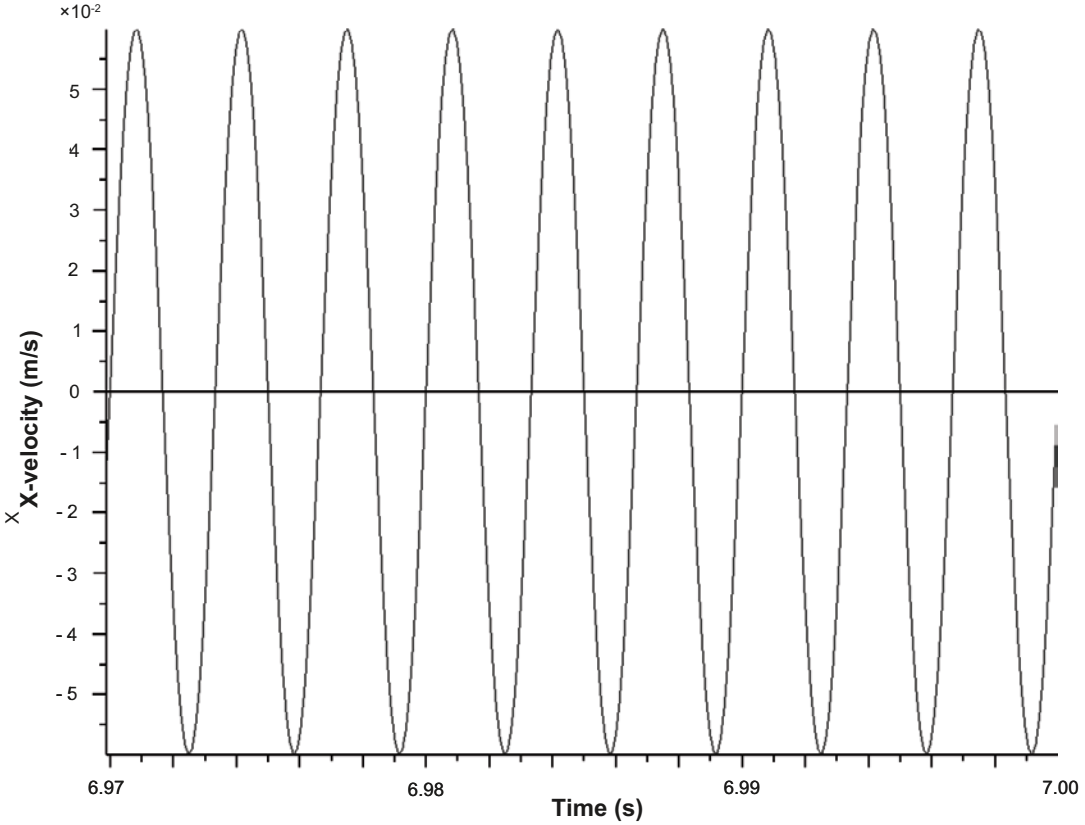

Figure 5-4. *Variation of velocity in X-direction versus time at point 1.*

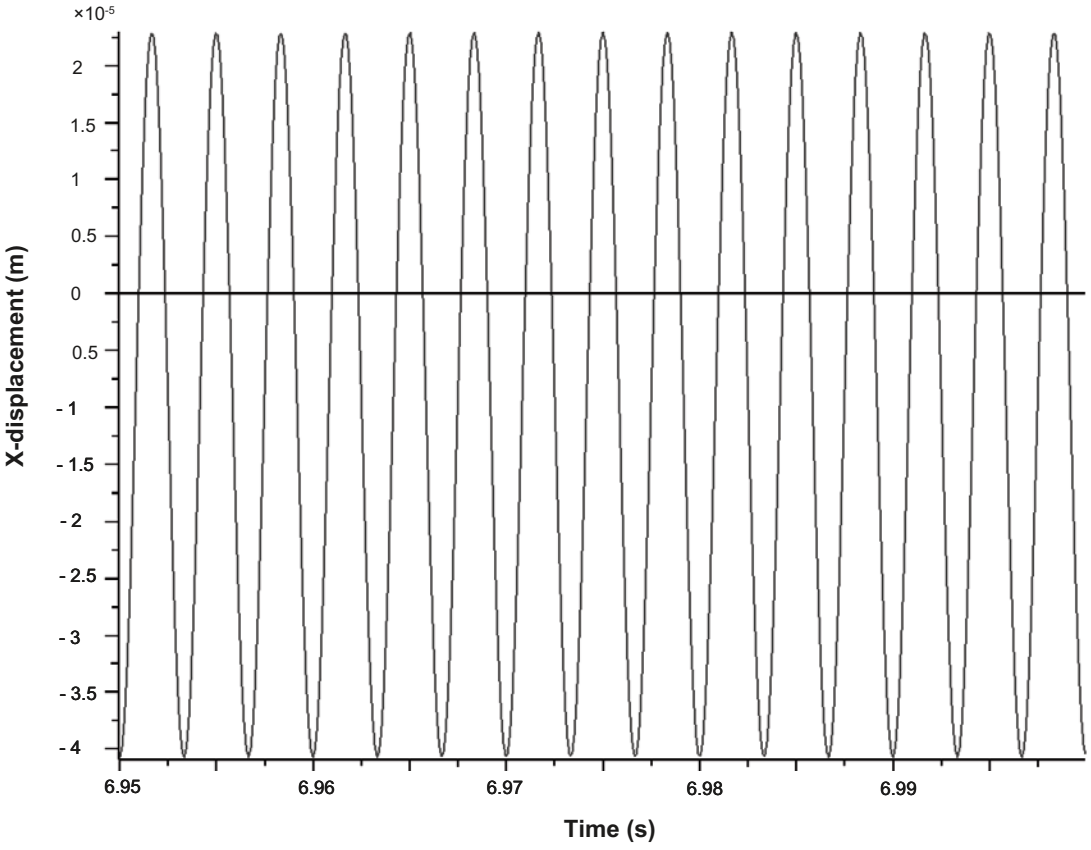

Figure 5-5. *Variation of displacement in X-direction versus time at point 1.*

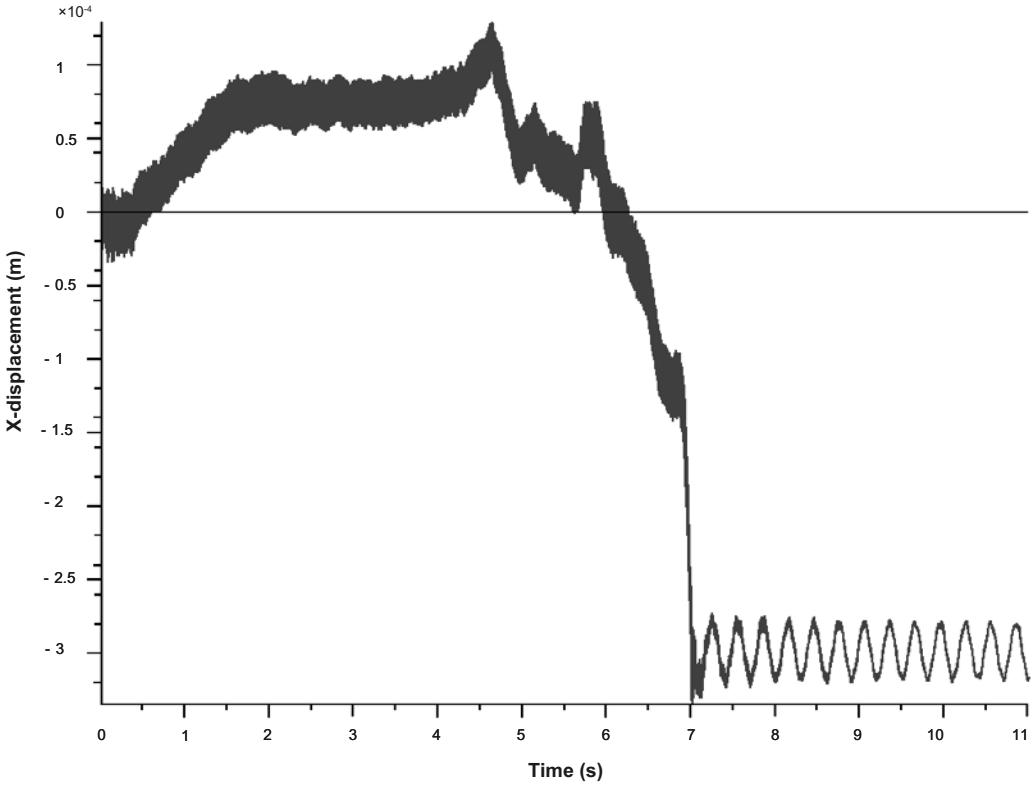

Figure 5-6. *Variation of X-displacement versus time at point 3.*

Table 5-4. Summary of the maximum displacements in contact planes for history points shown in Figure 5-3.

History point (see Fig. 5-3 for the location)	X-displacement (mm)
1	0.04
2	0.33
3	0.35
4	0.30
5	0.37
6	0.33
7	1.60

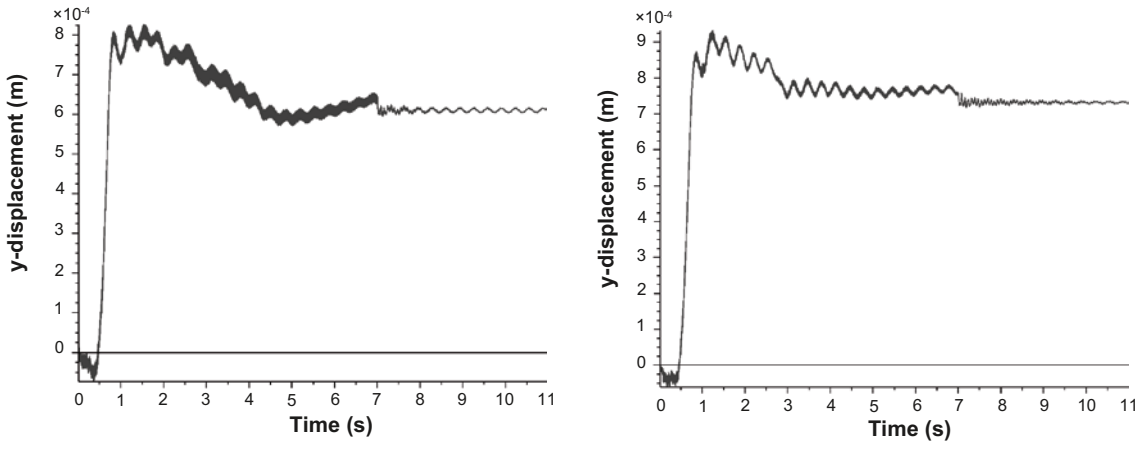

Figure 5-7. *Variation of X-displacement (left) and Y-displacement (right) versus time at point 3.*

As seen in Table 5-5, the combined effect of plane waves has increased both the X- and the Y-displacements. The maximum displacement occurs at the contact plane (history point 7) close to the top surface (Figure 5-3). The maximum calculated X- and Y-displacement is each 1.6 mm. The maximum particle displacement, which is the resultant of both X- and Y-displacement thus has increased.

5.2.3 Wave propagation in both X- and Z-direction

In this stage, the base case wave is combined with a wave propagating in vertical direction and is applied to the base of the column. As no information is available about the normal wave properties (phase-shift, amplitude etc) it was decided to apply the same wave properties for both X- and Z-direction. This assumption probably leads to comparatively higher X-displacements.

The history points were the same as for the base case, which is shown in Figure 5-3. Figure 5-8 shows the X-displacement and the Z-displacement for history point 3. The results for other points are given in Appendix 3.

As the excitation of the bentonite barrier is carried out in both X- and Z-direction, the X-displacement has considerably increased as expected. This behaviour can be explained when studying the shear force in the contact plane. As the two planes lose their contact, also the shear force which constrains movements vanishes. As seen in Figure 5-8, the X-displacement at history point 3 has increased to 26 mm compared to previous combinations as shown in Figure 5-6.

Table 5-5. Summary of the maximum X- and Y-displacements in contact planes.

History point (see Figure 5-3 for the location)	X-direction (mm)	X-direction (mm)
1	0.04	0.05
2	0.78	0.08
3	0.80	0.09
4	0.82	0.09
5	0.92	0.09
6	0.96	0.10
7	1.60	1.45

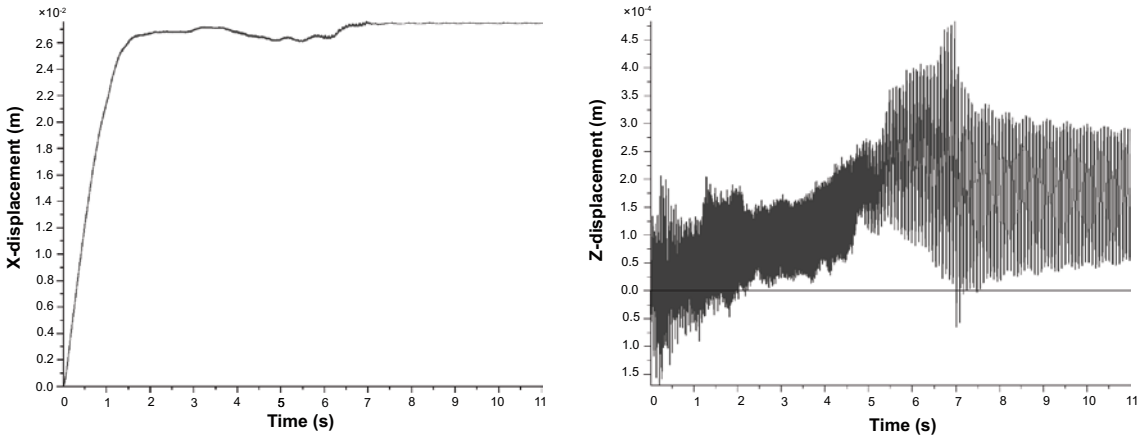

Figure 5-8. *Variation of X-displacement (left) and Z-displacement (right) versus time at point 3.*

5.3 Sensitivity analysis

5.3.1 Elastic modulus

The elastic modulus of the bentonite material was provided by Clay Technology and ranged from 300 to 600 MPa /Johannesson 2008/. In our analysis the base case study was carried out with 300 MPa. In order to investigate the effect of higher value, the elastic modulus was set to 600 MPa in a next analysis. The displacement of the contact planes, were monitored at points 2–7 (see Figure 5-3). A typical behaviour of X-displacement in contact plane 3 is presented in Figure 5-9. The displacements for the other contact planes are given in Appendix 4.

The results show that bentonite rings with a higher elastic modulus, which means that they are stiffer, displays much less compared to the base case – where 300 MPa was used.

5.3.2 Friction angle

The properties of the contact plane play an important role during the excitation to prevent any movements between the rings. The frictional resistance force is a function of the vertical load (gravity) and the friction angle. According to Clay Technology /Johannesson 2008/ a variation of the friction angle between 10° and 20° can be expected. In the study of the base case, it was decided to investigate the influence of the friction angle when lowering its value to 10° (as the base case was carried out by using 15°, a reasonable assumption is made here that higher friction angle causes lower movement in the contact planes. Thus, 20° was not taken into consideration). In Figure 5-10, the X-displacement versus time is given for history point 3. In Appendix 5, the displacements for all history points are shown.

The summary of maximum displacements is given in Table 5-6. The maximum displacement occurs at the contact plane 7, which is the same as for the base case. The maximum X-displacement is 1.4 mm. X-displacement at the base level (history point 2) is about two times higher than the base case. It can be observed that displacements at all the contact planes have increased compared to the base case. The major reason for this is that the shear-force in the contact plane is a function of the friction angle. A reduction of the friction angle used between the contact planes cause a reduction of the shear force, which then give a larger movement.

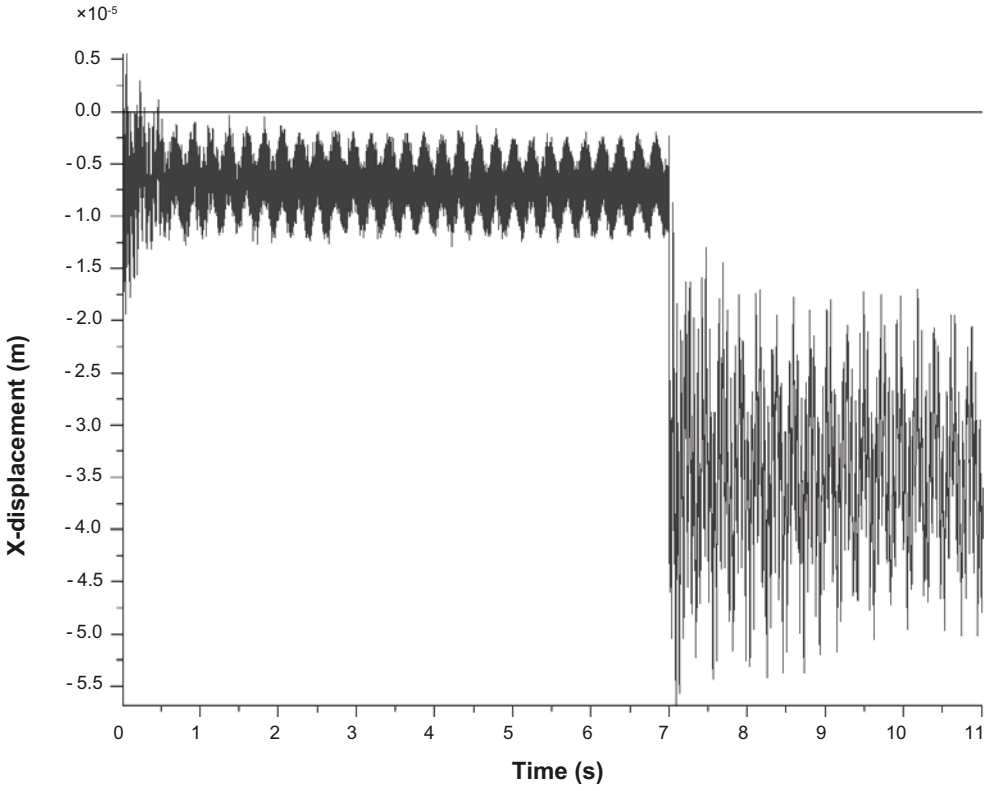

Figure 5-9. *Variation of X-displacement versus time at point 3.*

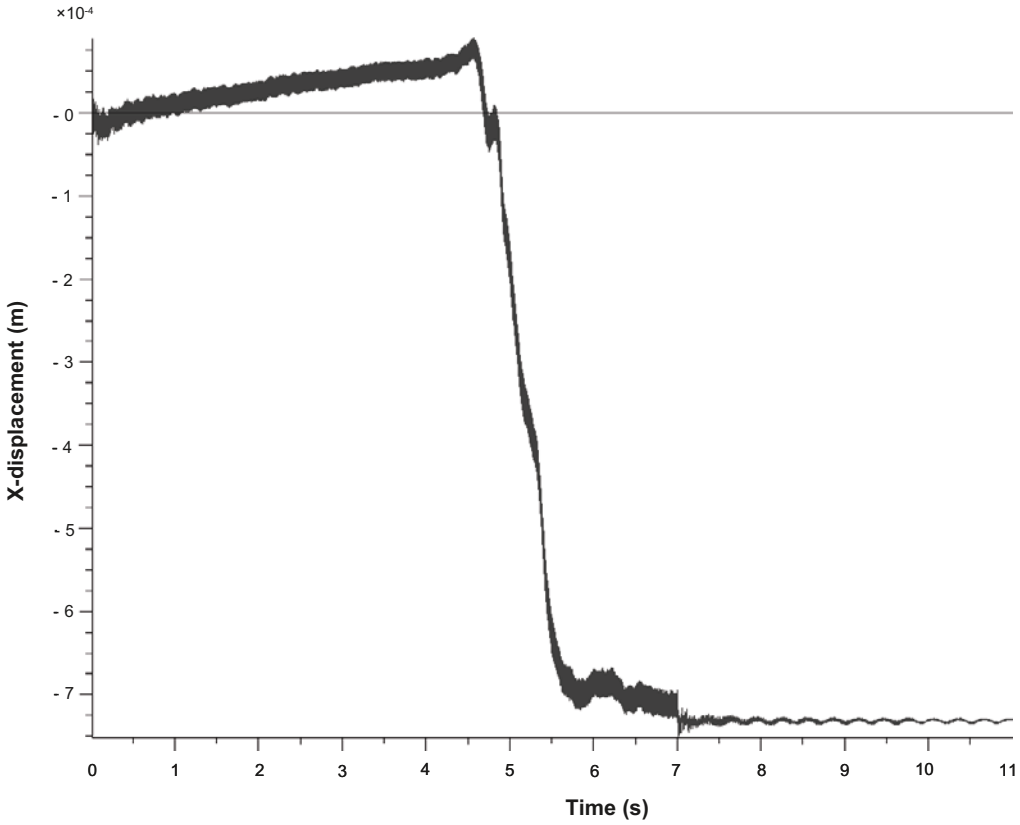

Figure 5-10. *Variation of X-displacement versus time at point 3.*

Table 5-6. Summary of the maximum X-displacement in the contact planes with friction angle 10°.

History poin (See Figure 5-3 for the location)	X-displacement (mm)
1	
2	0.72
3	0.72
4	0.70
5	0.70
6	1.00
7	1.40

5.3.3 Resonance frequency

Any physical system tends to oscillate with its maximum amplitude at the resonance frequency. At this frequency, small amplitudes of the wave can cause a large displacement in bentonite rings. Due to this reason, it is important to examine the responses of the bentonite barrier when the wave is applied with a frequency that matches the frequency of the structure. In order to study the above effect, the resonance frequency was determined analytically assuming a fix boundary condition and a continuous structure (see section 3.2.2). From this analytically solution, it was concluded that the natural frequency for the system was about 9 Hz. Thus, the frequency for this analysis was 9 Hz. The amplitude was selected to 0.06 m as for the base case. In Figure 5-11, the X-displacement for history point 3 is illustrated. The results for other history points are shown in Appendix 6.

In contrast to the previous cases, a rapid variation of X-displacement can be observed at point 3, which has a maximum displacement of 2.25 mm. Even though this is marginally higher than the previous cases, no significantly higher variation of X-displacement at point 3 due to natural frequency was observed. One possible reason for this may be the assumptions used when deriving the natural frequency.

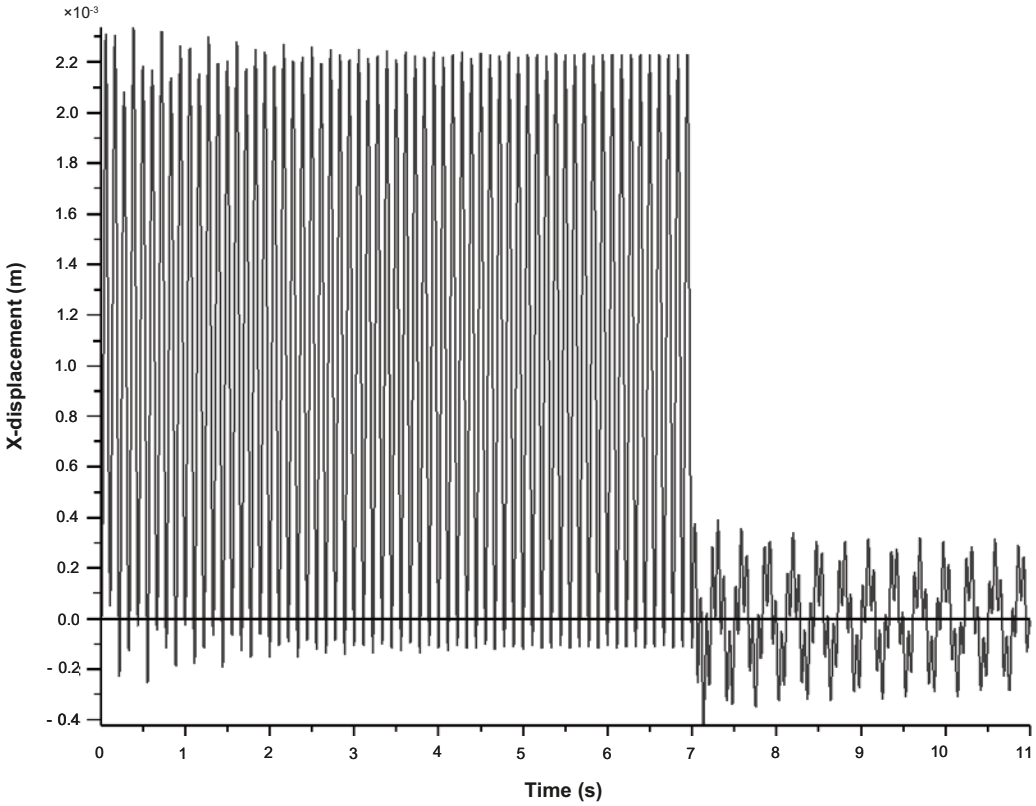

Figure 5-11. *Variation of X-displacement versus time at point 3.*

5.4 Sampled blasting wave applied to the bentonite rings

The experience of researchers /Chen and Zhao 1998/ shows that the blasting induced waves are very different to the sinusoidal or triangular time dependant load. When the sinusoidal time dependant load is used, a vibration signal with amplitude and an approximated frequency is applied to the system. For the base case, a frequency of 300 Hz and amplitude of 60 mm/s was applied as the dynamic load at the bottom of the bentonite rings. In the real case, the vibration signal is quite different as the maximum amplitude occurs only at a single time throughout the considered period. Although a sinusoidal approach provides a good starting point, it is believed that the results are conservative.

Considering the above mentioned facts, it was decided to apply a recorded vibration signal generated from blasting activities in TASS tunnel. This signal was provided by SKB from measurements carried out by Bergsäker AB and originates from vibration measurements performed in vertical direction close the BTG plug. The signal was sampled with 3 kHz and no measurements were carried out in the horizontal direction. As the original signal had amplitude that was much lower than the stipulated value of 60 mm/s used for the previous analysis, the amplitude of the original signal had to be scaled. Using this approach, only the amplitude will be changed whereas the frequency content in the signal will be maintained. It can be noticed the measured wave is quite different to the approximated sinusoidal wave or triangular.

As 3DEC can read time dependant properties such as velocity and stress in table form for both regular and irregular time intervals, velocity histories were given to 3DEC as the original table. The scaled vibration signal used for this analysis can be seen in (Figure 5-12). As the maximum X-displacement observed was about 23 mm for the combined sinusoidal waves in X- and Z-direction, it was decided to study the combined wave effect in detail with the measured waves. For this simulation, it was assumed that the phase shift was zero (the maximum in both directions occur at the same time). As no measurements were done in horizontal direction, identical waves (vertical measured wave) were applied in both and directions.

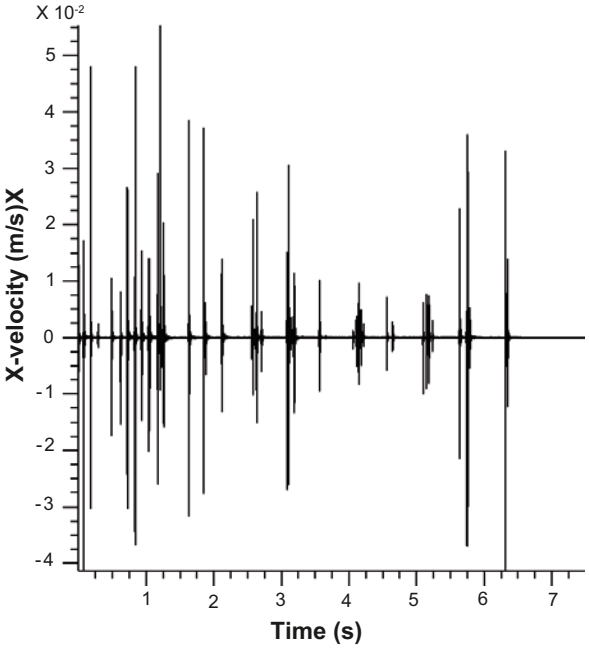

Figure 5-12. *3DEC generated X-velocity versus time at point 1.*

Before studying the results obtained from the simulations, is it essential to verify that the correct boundary conditions are applied to the model. This was done by comparing the input signal in 3DEC and the measured signal. In Figure 5-12, the 3DEC generated X-velocity at location 1 is shown.

The history monitoring points were the same as for the base case (Figure 5-2). In Figure 5-13, the X-displacement for history point 3 can be seen. The results for the other points are presented in Appendix 7.

As seen in Figure 5-13, the maximum X-displacement that occurs after 7 seconds is about 0.34 mm. From the starting point up to two seconds, the displacement increases in two steps. After two seconds, a gradual rise of the displacement up to 6.5 seconds can be observed. However, after the first 6.5 seconds, the displacement gradually approaches to a constant value. In Table 5-7, a comparison of the displacements in X-direction at point 3 due to approximated sinusoidal wave and the real wave is shown.

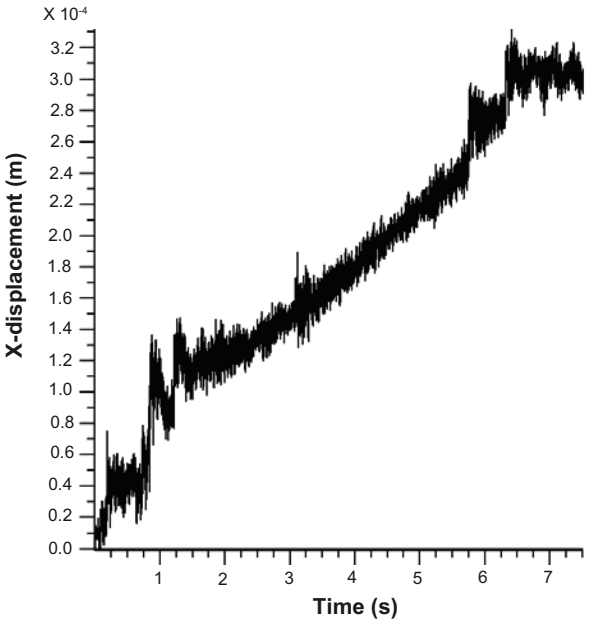

Figure 5-13. *Variation of X-displacement versus time at point 3.*

Table 5-7. Comparison of the maximum X-displacement in contact planes.

History point (see Figure 5-3 for the location)	X-displacement (sinusoidal) (mm)	X-displacement (real wave) (mm)
2	24	0.32
3	26	0.34
4	27	0.32
5	26	0.30
6	26	0.32
7	23	0.36

As shown in Table 5-7, the X-displacement related to the real wave is about 98.6% lower than the X-displacement produced by the approximated sinusoidal wave. It is believed that the above mentioned difference occurs mainly due the differences in the input wave properties. In the idealised sinusoidal approach, a wave with the amplitude of 60 mm/s and the frequency 300 Hz is applied during the period of 6 seconds. However the analysis of real wave shows that the maximum amplitude 60 mm/s occurs only at one time during the period of 7 seconds and most of the time, the applied amplitude is less than 10 mm/s. Therefore it can be reasonably assumed that the idealised sinusoidal wave carries more energy to bentonite rings compared to the real wave, thus making the system to move more.

6 Discussion and conclusions

During the construction of a final repository for spent nuclear fuel in crystalline rock, some of the blasting activities in certain deposition tunnels may take place at the same time as the deposition of canisters containing the waste. Considerations about blasting in the vicinity of a sealed deposition hole have shown that there should not be any risk for the functionality and safety of the deposition. Furthermore, the canister itself would not be affected by the blasting vibrations due to the much harder requirements on its design, material, and construction. On the other hand, it seems that the most critical period of time; from a vibration point of view, is when the bentonite buffer is placed in the deposition hole but the canister.

A preliminary evaluation indicates that a distance between the blasting and a deposition hole shorter than 80 m could jeopardize the integrity of the buffer. To guarantee that the level of vibration after the positioning of the buffer is not too high, it has been assumed that the blasting cannot take place closer than two deposition tunnels away from the buffer. However, this study was aimed to determine more in detail the displacements on the buffer when exposed vibrations outgoing from an analyses that take into account the velocity and frequency contents of the vibration, the geometry of the problem and the material properties of rock mass and bentonite. For this purpose, the three dimensional discrete element code (3DEC) was used. The waves generated by nearby blasting were approximated to a sinusoidal wave in the first phase of the study and in the second phase, a measured vibration signal was used.

The movements of the contact planes were first studied with the sinusoidal wave component applied only in the X-direction (X- and Y-waves are in the horizontal plane whereas Z waves in the vertical plane). The maximum displacement occurs at the uppermost contact plane with the value of 1.6 mm. In the next step, when the vibrations signal was applied in both X- and Y-directions, the displacement increased in all the contact planes and the maximum displacement occurred at the upper most contact plane with the value of 2.02 mm.

In order to study the effect of the vertical vibration applied to the system, one simulation was done with both vertical and horizontal components. As no specific data on the vertical component of the propagating wave was available, it was assumed that this component had the same magnitude as for the X- and Z-directions. This analysis then included two wave components (one horizontal and vertical) that resulted in a displacement at the uppermost plane of 22.03 mm. This is significantly larger than the displacements with only one or two components of the propagated wave when applied only in the horizontal direction. The assumption used in this study – where a sinusoidal signal without any phase shift is used is believed to be conservative.

The final step within this study was to investigate the assumption of a sinusoidal vibration signal. Therefore, one simulation was carried out with a measured vibration signal. When combining the X- and Z-waves and using the measured vibration signal significantly lower displacement were observed between the contact planes. For this analysis the maximum displacement occurred in the uppermost plane with the maximum value of 0.35 mm. Thus it can be concluded that the approach with a sinusoidal vibration signal is very conservative.

The effect of material properties was studied by carrying out a number of analysis with the sinusoidal wave component only in X-direction. Analysis with the friction angle of 10° shows that displacement increased marginally at all contact planes (i.e. the X-displacement at the lower most plane, history point 2, is 0.70 mm whereas in the base case it is 0.35 mm). As the base case was simulated with the lowest modulus of elasticity (E = 300 MPa), sensitivity analysis including higher elastic modulus always reduced displacements in all contact planes. The maximum displacement obtained with elastic modulus E = 600 MPa was 0.02 mm at the upper most contact plane, which is much lower than the displacement corresponding to the elastic modulus of 300 MPa.

Our results are useful when deciding the distance to a new blasting location from an existing repository. One encouraging implication of the results when simulating the real wave is that the blasting generated waves do not cause significant movements in the bentonite rings when using 4 kg as the charge and assuming a distance of 30 meters between the blast and the buffer. However, it should be noted that the confidence in results can be further enhanced by numerically simulating all the three measured velocity components of the wave at the bottom of bentonite rings.

7 References

Andersson A, 2003. Aspö Pillar Stability Experiment. Summary of preparatory work and predictive modelling. SKB R-03-02, Svensk Kärnbränslehantering AB.

Bachmann H, Ammann W, 1987. Vibrations in Structures Induced by Man and Machines. Structural Engineering Document 3e, Int. Assoc. for Bridge and Structural Engineering, IABSE-AIPC-IVBH, Zurich. ISBN 3-85748-052-X.

Bodare A, 1997. Kompendium i Jord och Bergdynamik 1B1435, Institute for Soil and Rock Mechanics, Royal institute of technology.

Chen S G, Zhao J, 1998. Study of UDEC Modelling for Blast Wave Propagation in Jointed Rock Masses, International Journal of Rock Mechanics and Mining Sciences. 35, pp 93–99.

Fredriksson A, Johansson S-E, Niklasson B, 2004. Inkapslingsanläggning – Byggbarhetsanalys av bergschakt. SKB R-04-06, Svensk Kärnbränslehantering AB.

Johannesson L E, 2008. Personal communication. Clay Technology AB.

Itasca Consulting Group Inc, 2008. 3DEC version 4.1, Minneapolis, USA.

Nyberg U, Harefjord L, Bergman B, Christiansson R, 2005. Monitoring the vibrations during blasting of the TASQ tunnel. SKB R-05-27, Svensk Kärnbränslehantering AB.

Lindman S-O, Lönnblad C, Palmer S, 2007. Projektering slutförvar – Referensutformning för slutförvarsanläggningen. PIR-07-22, Svensk Kärnbränslehantering AB.

Svensk Standard SS 460 48 66, 1991. Vibration och stöt – Riktvärden för sprängningsinducerade vibrationer i byggnader**.**

Wersäll C, 2008. Blast-Induced vibrations and stress field changes around circular tunnels. Master of thesis, Institute for Soil and Rock Mechanics, Royal institute of technology.

Appendix 1

Plane wave in X-direction

History points

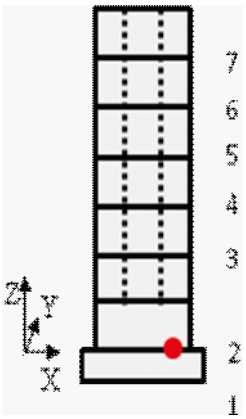

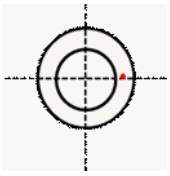

X-Displacement (m) Vs Time (s)

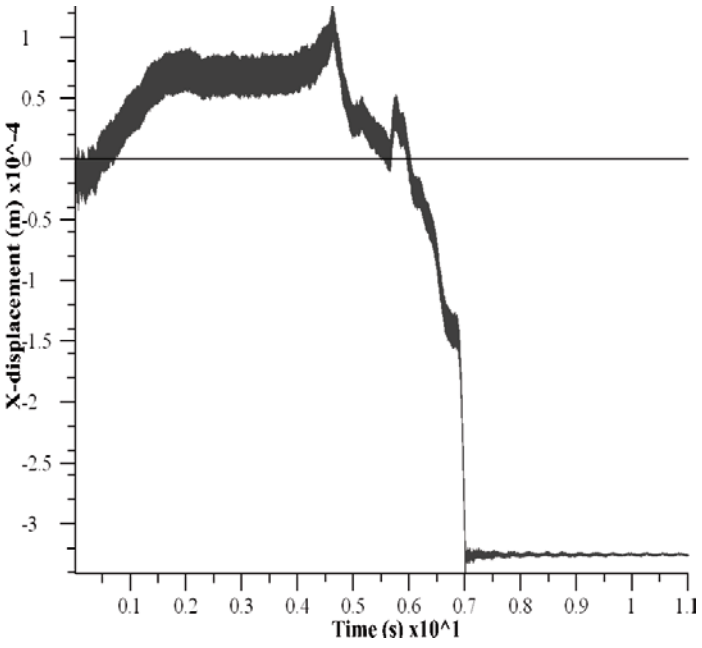

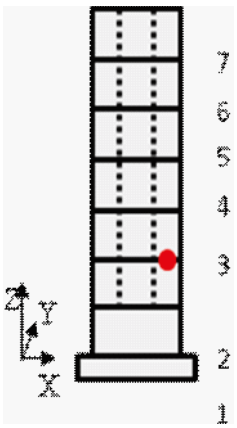

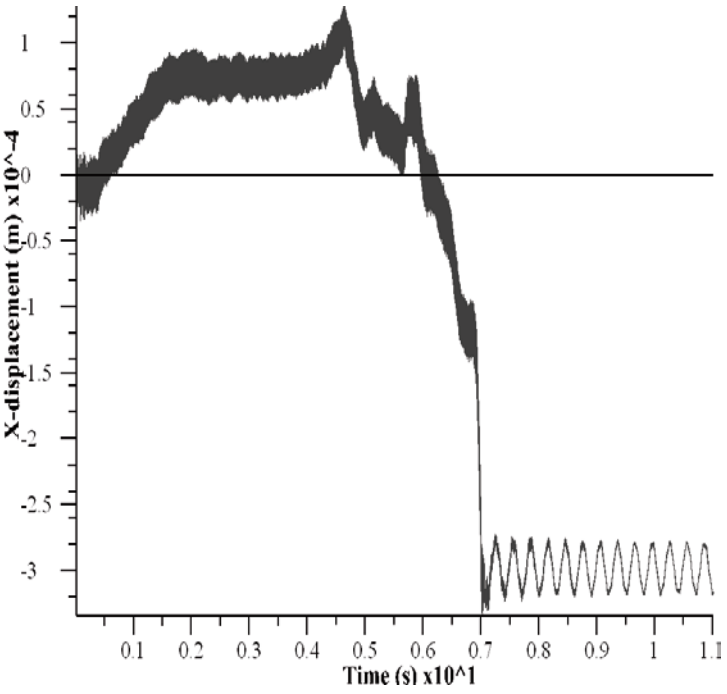

History points

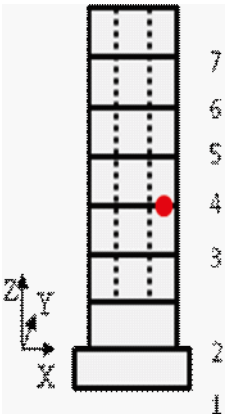

X-Displacement (m) Vs Time (s)

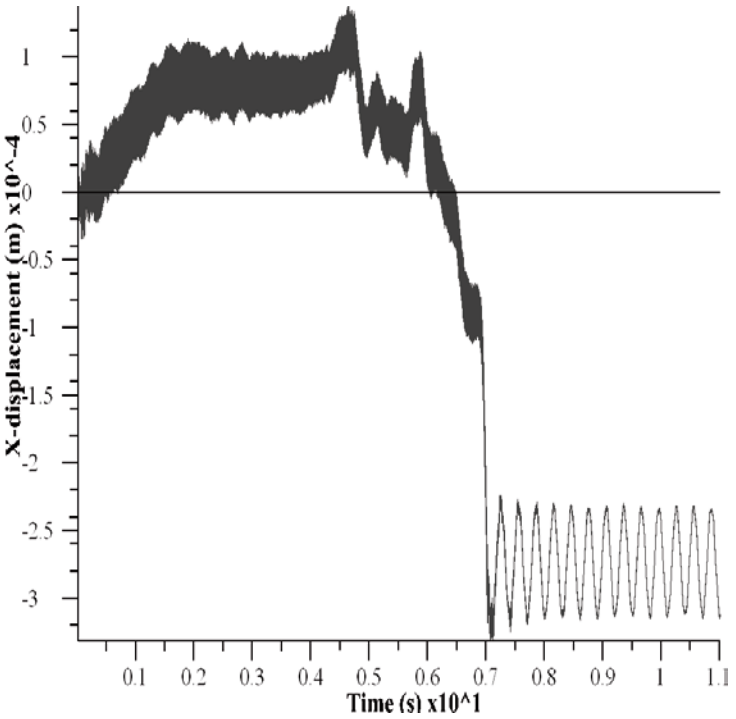

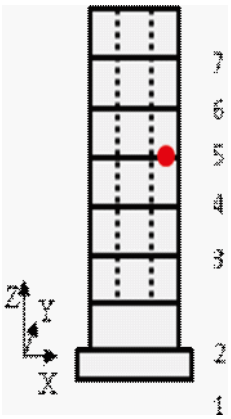

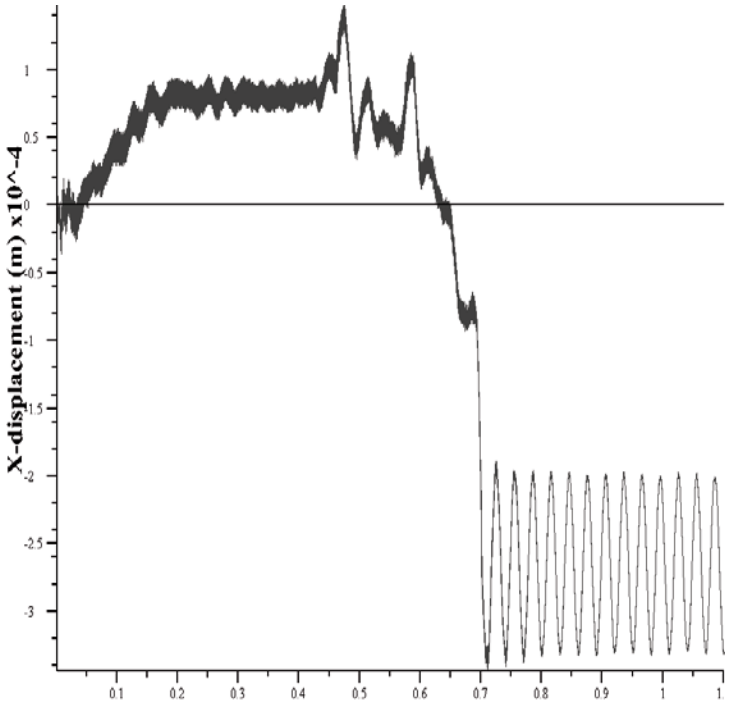

History points

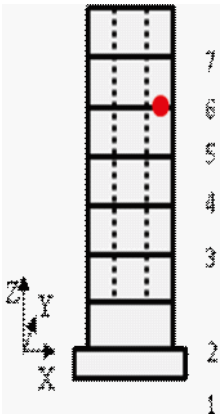

X-Displacement (m) Vs Time (s)

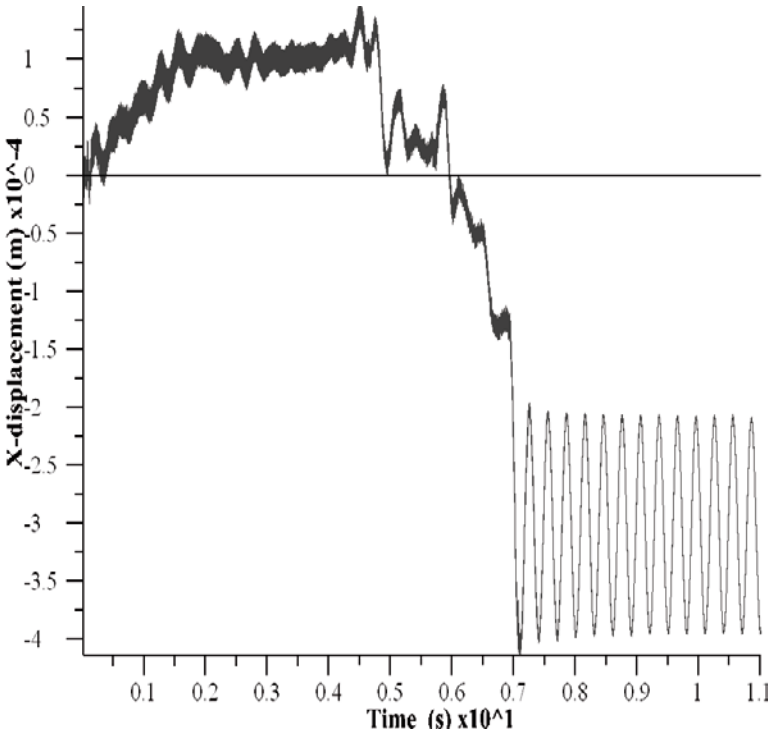

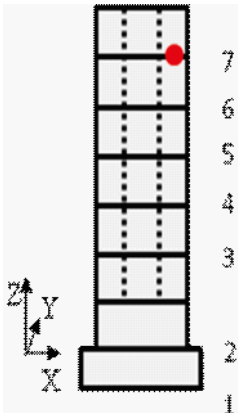

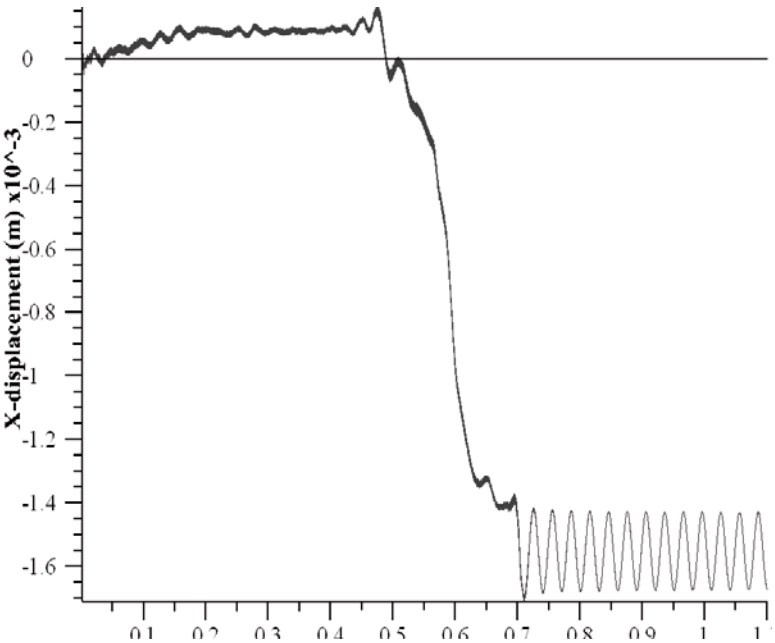

Appendix 2

Plane wave in X- and Y-direction

History point

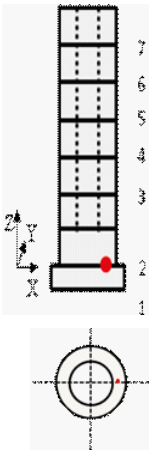

X-Displacement (m) Vs Time (s)

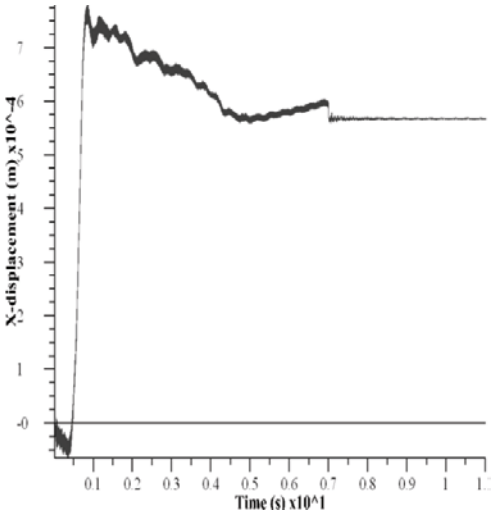

Y-Displacement (m) Vs Time (s)

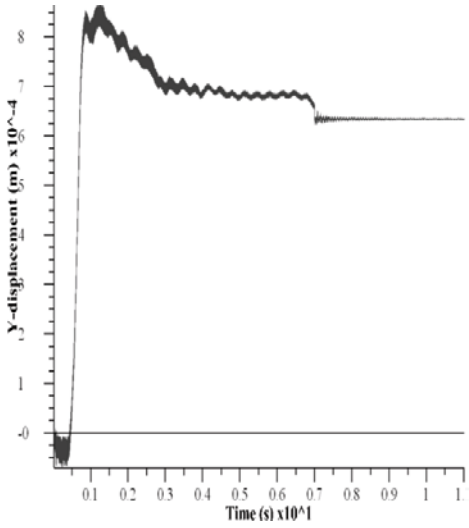

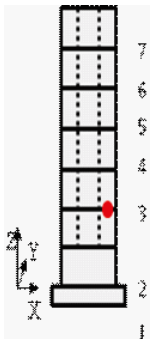

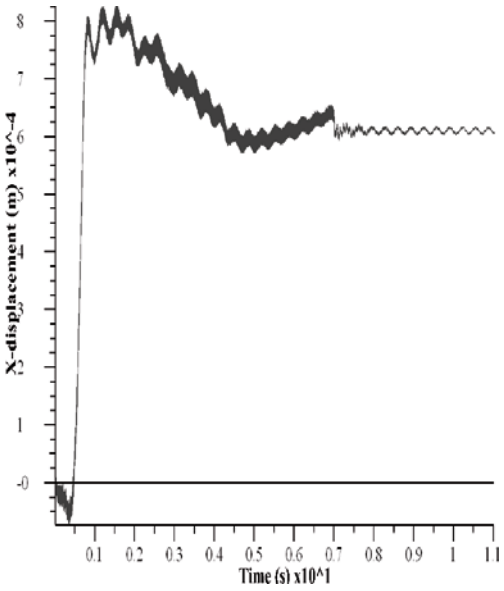

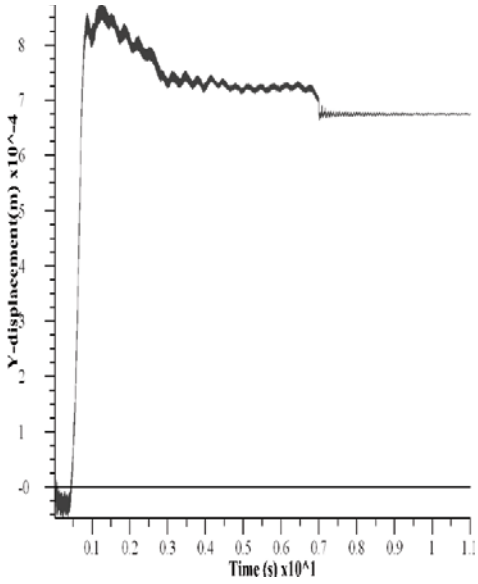

History point

X-Displacement (m) Vs Time (s)

Y-Displacement (m) Vs Time (s)

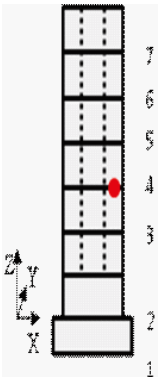

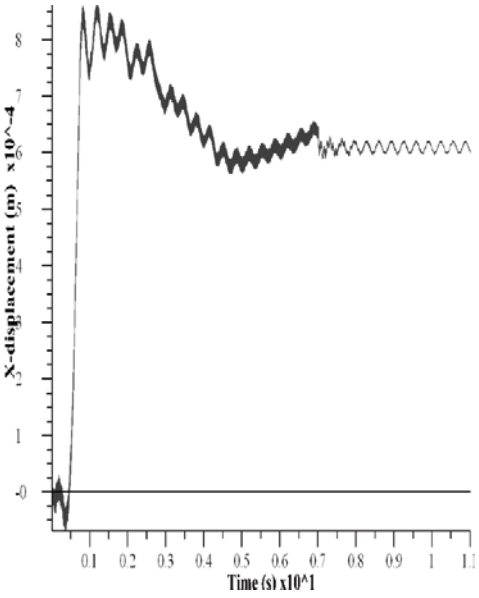

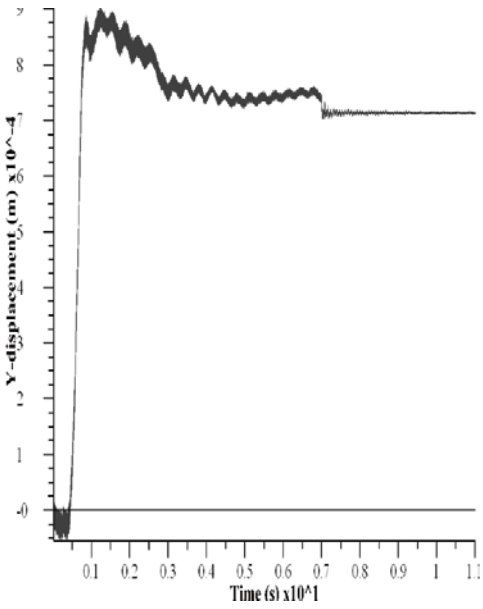

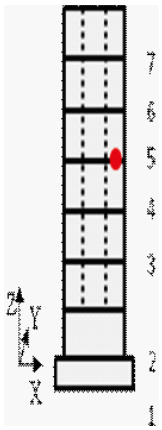

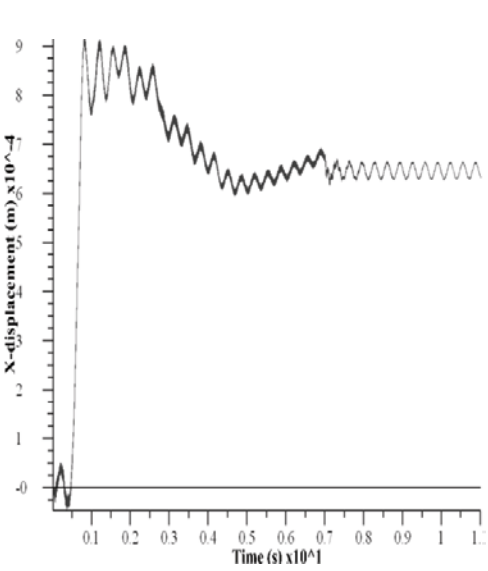

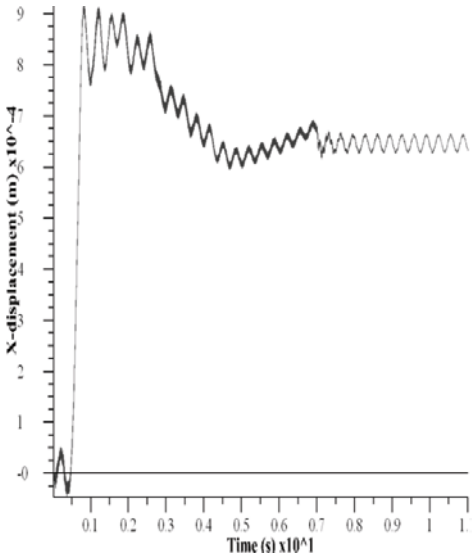

History point	X-Displacement (m) Vs Time (s)	Y-Displacement (m) Vs Time (s)
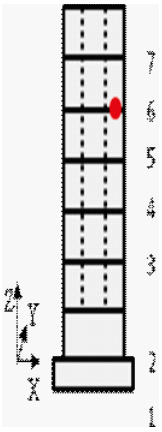	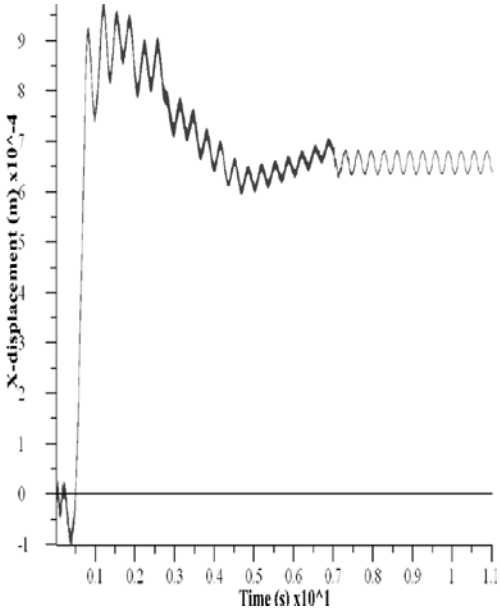	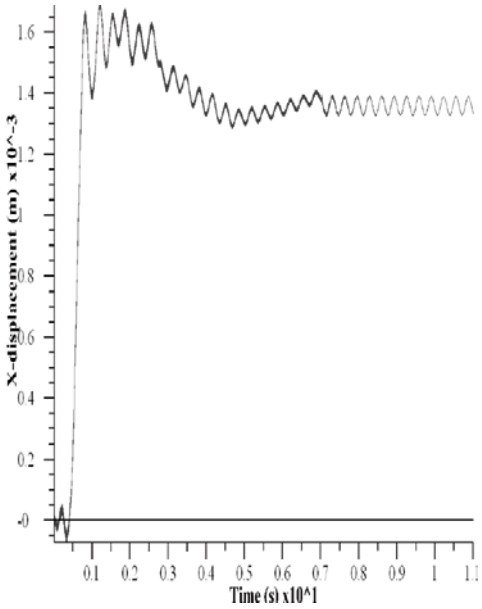
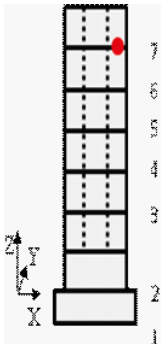	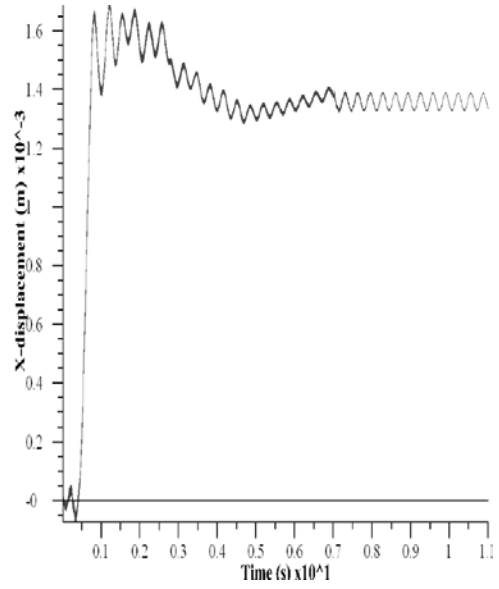	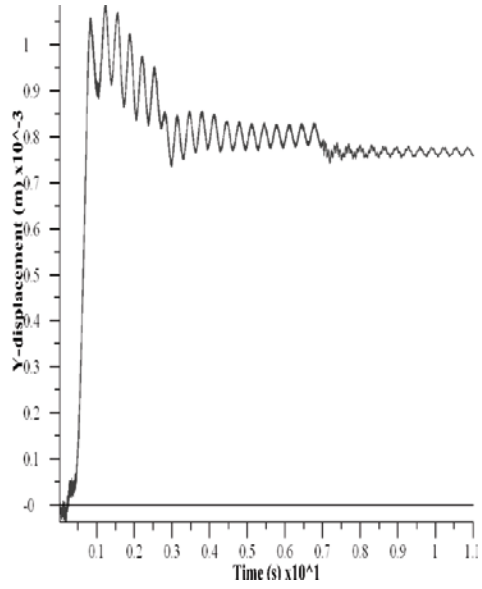

Appendix 3

Plane wave in X- and Z-directions

History point

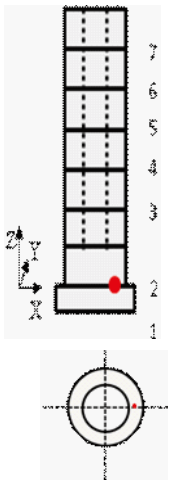

X-Displacement (m) Vs Time (s)

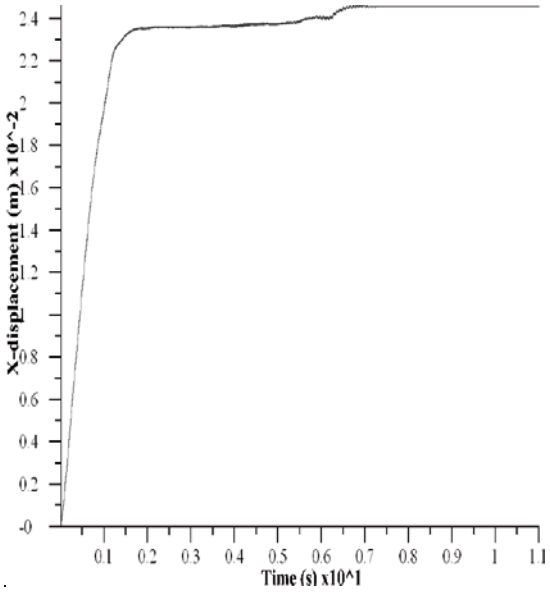

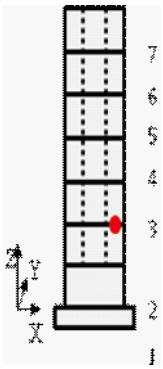

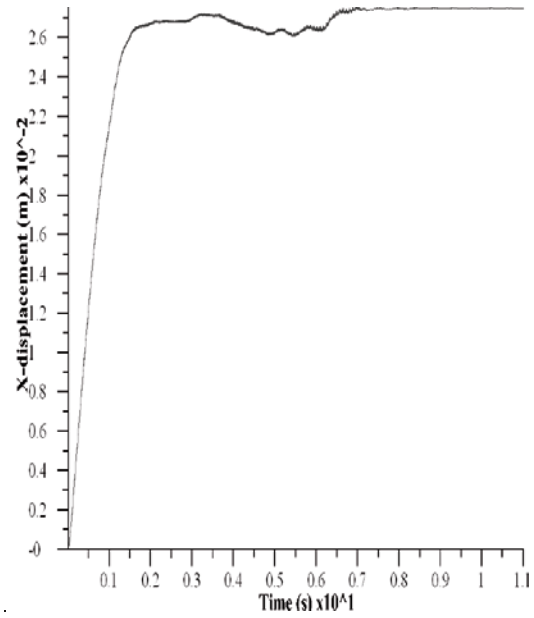

History point **X-Displacement (m) Vs Time (s)**

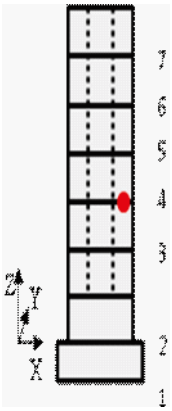

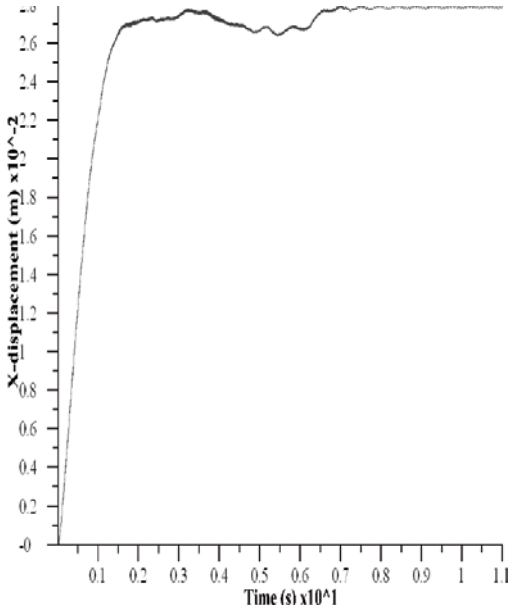

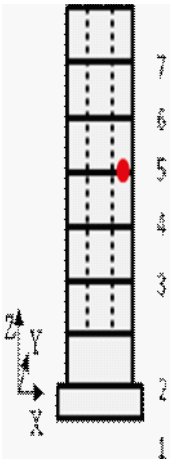

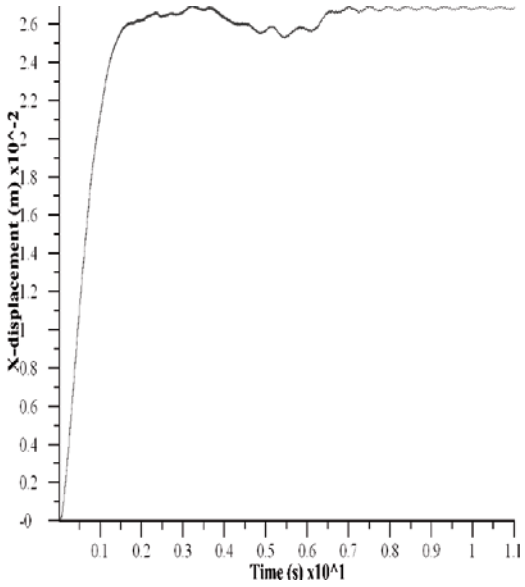

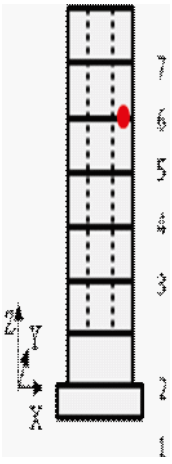

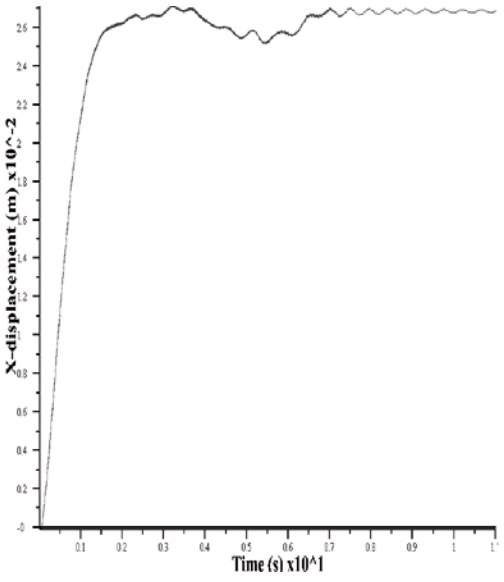

History point

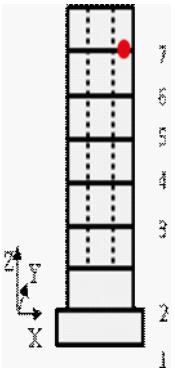

X-Displacement (m) Vs Time (s)

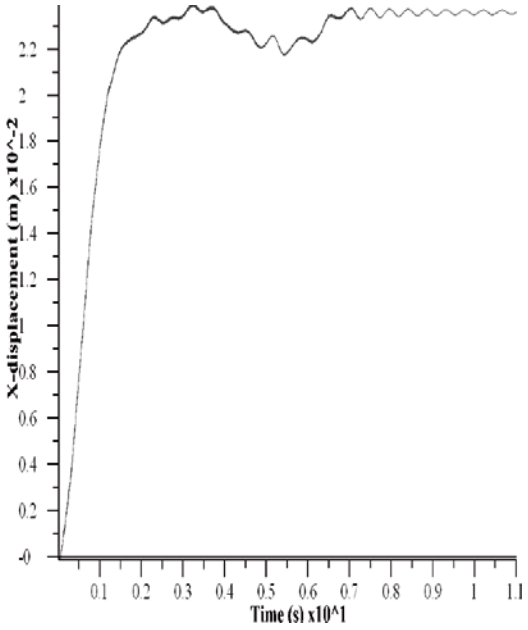

Appendix 4

Sensitivity analysis of the E-modulus

History point

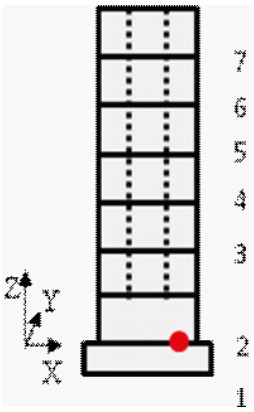

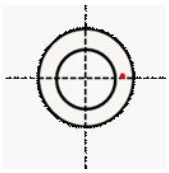

X-Displacement (m) Vs Time (s)

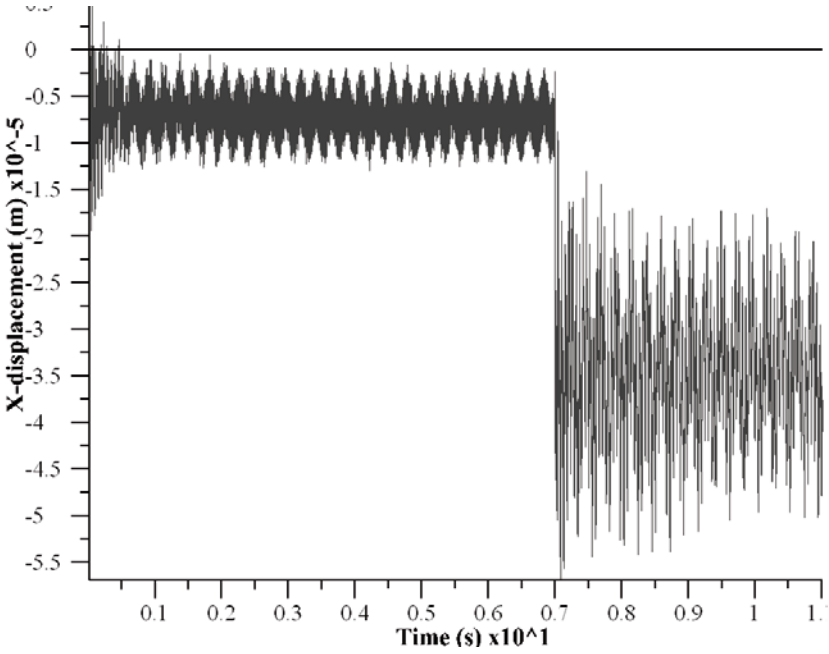

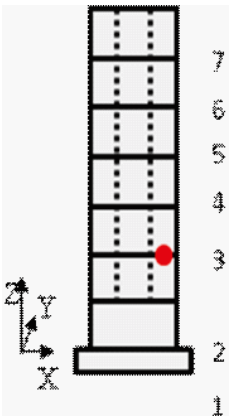

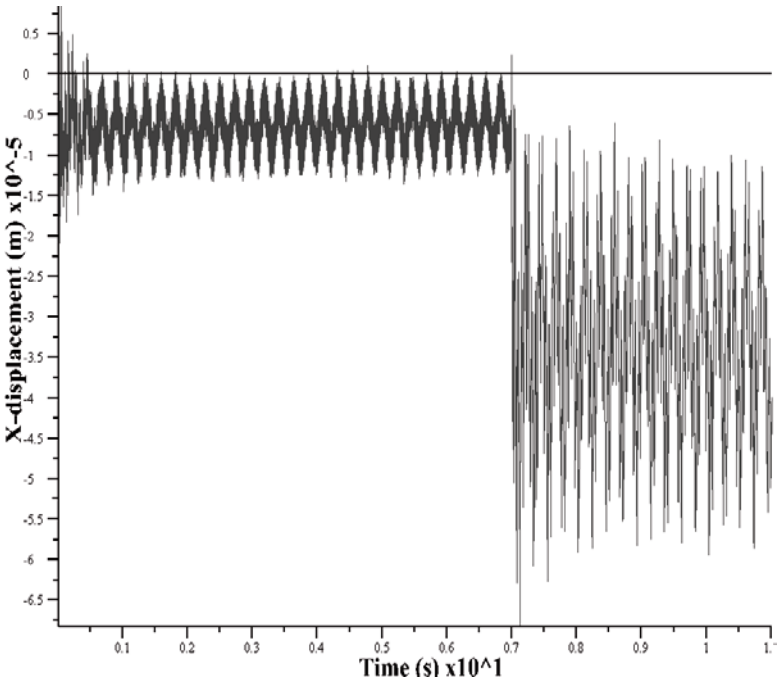

History point

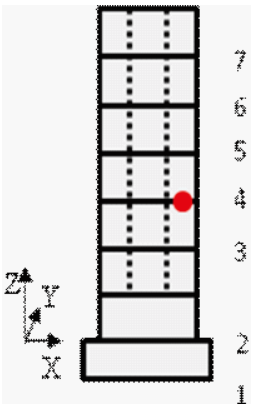

X-Displacement (m) Vs Time (s)

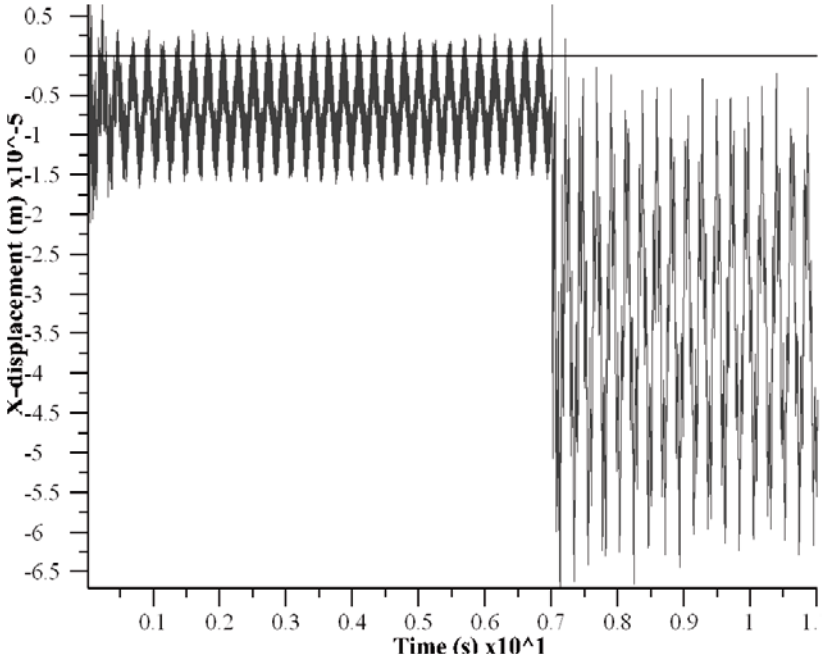

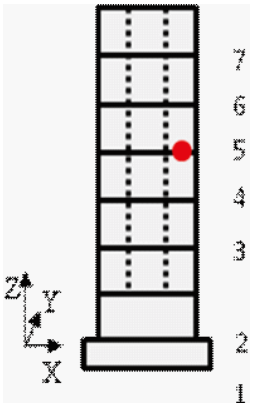

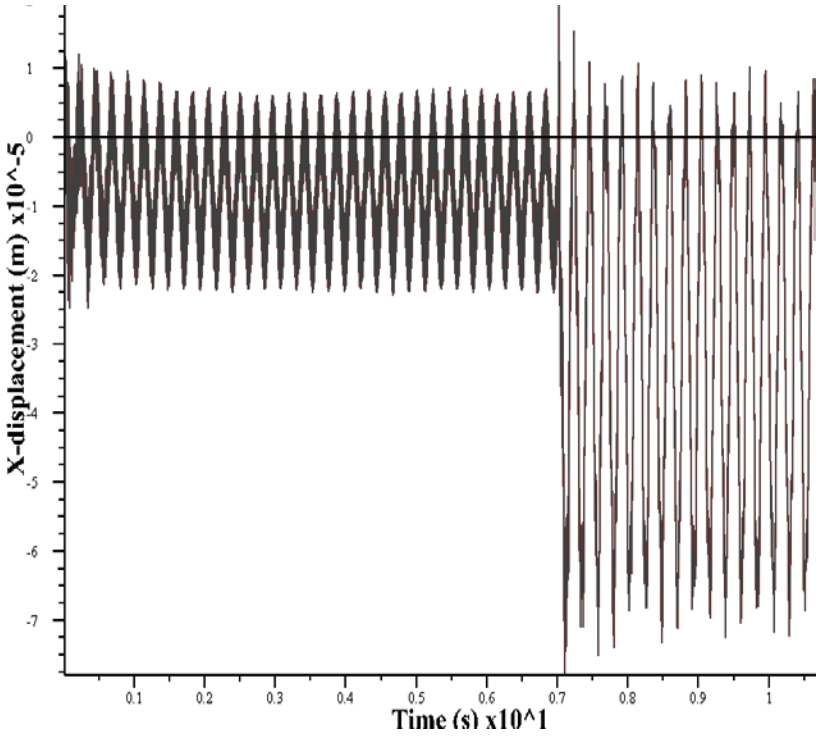

History point

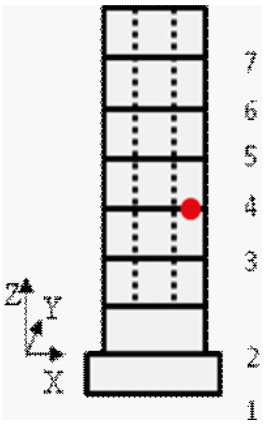

X-Displacement (m) Vs Time (s)

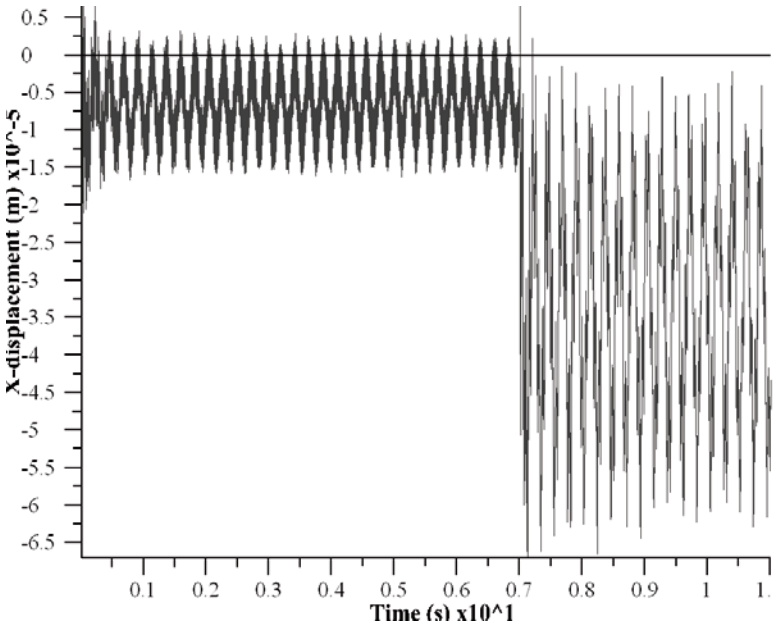

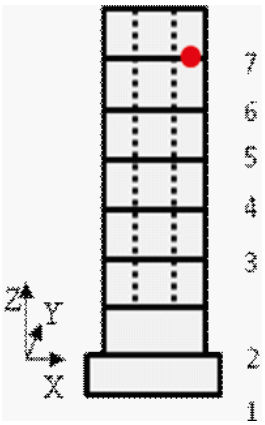

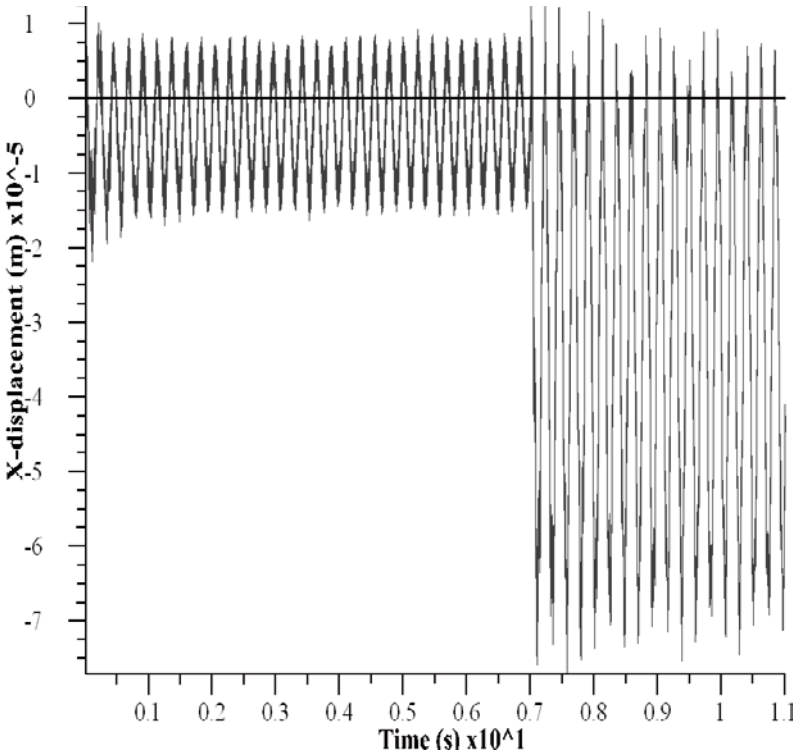

Appendix 5

Sensitivity analysis of the friction angle

History point

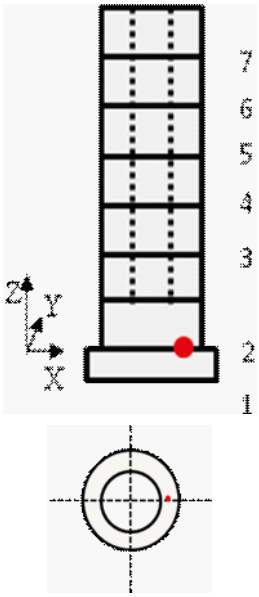

X-Displacement (m) Vs Time (s)

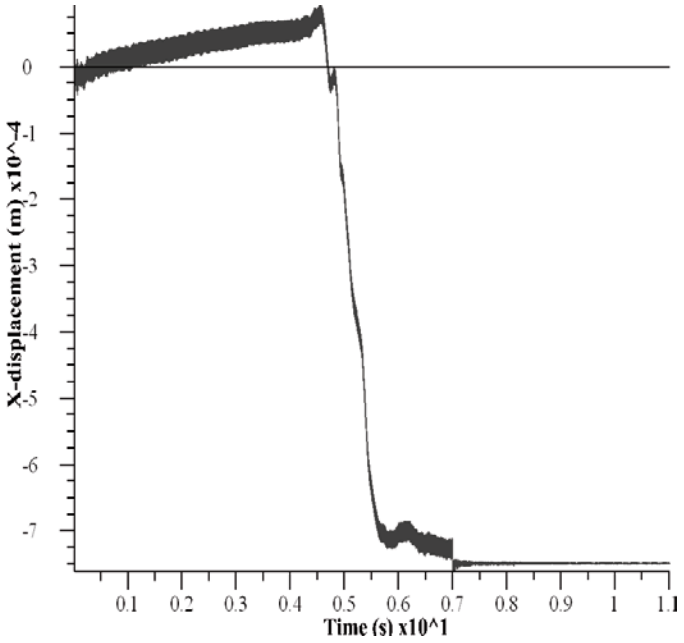

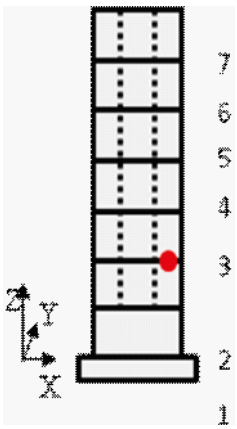

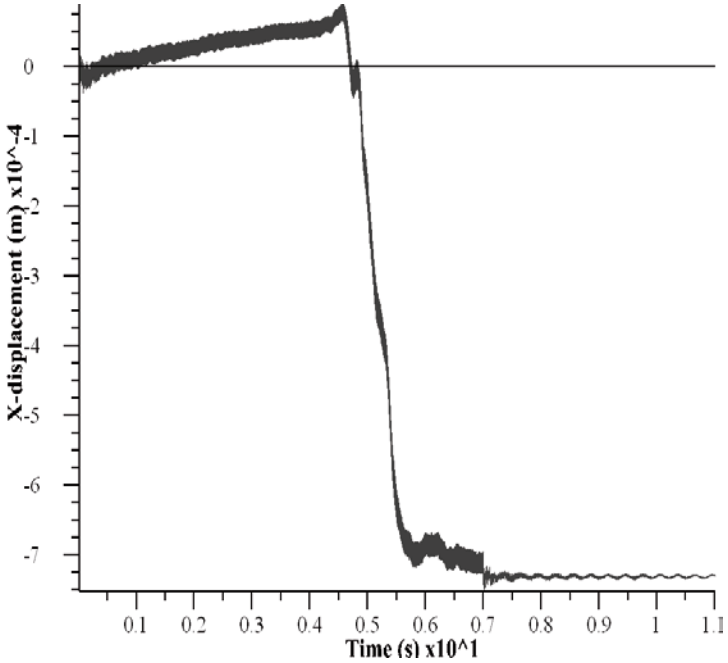

History point

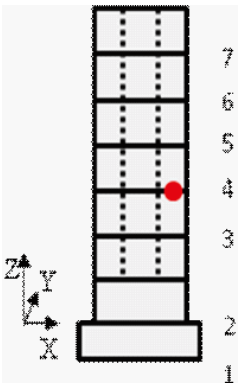

X-Displacement (m) Vs Time (s)

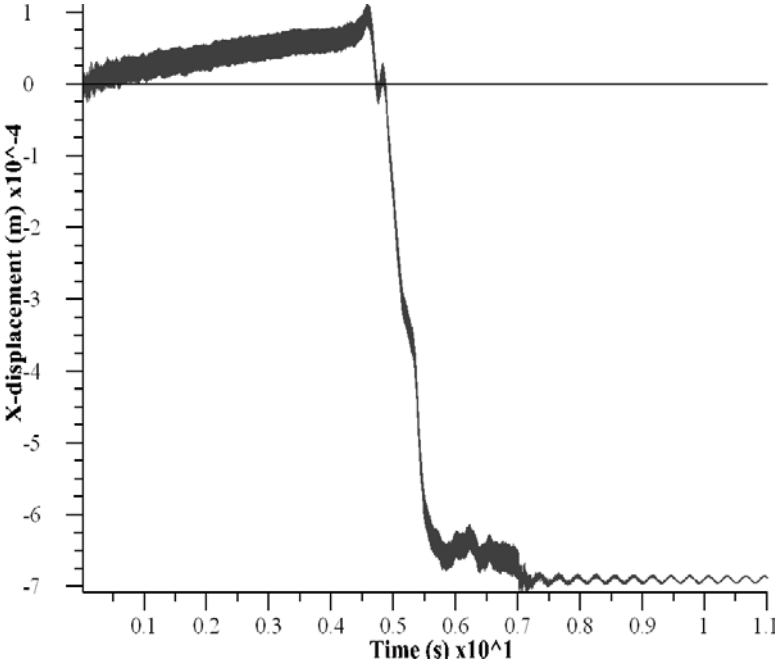

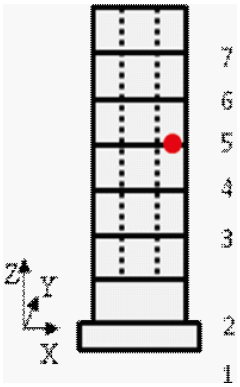

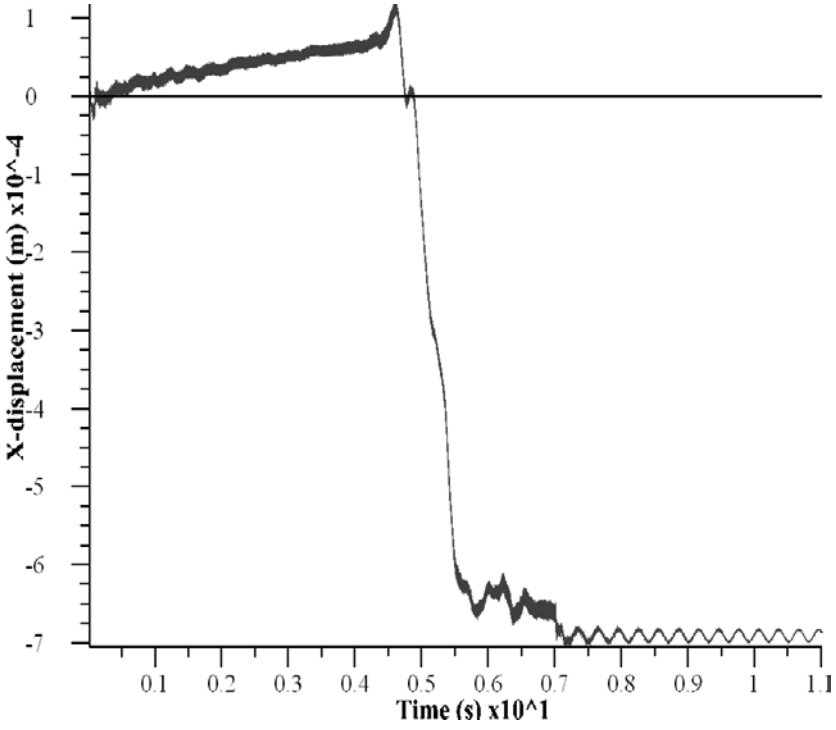

History point

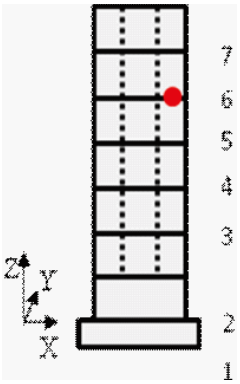

X-Displacement (m) Vs Time (s)

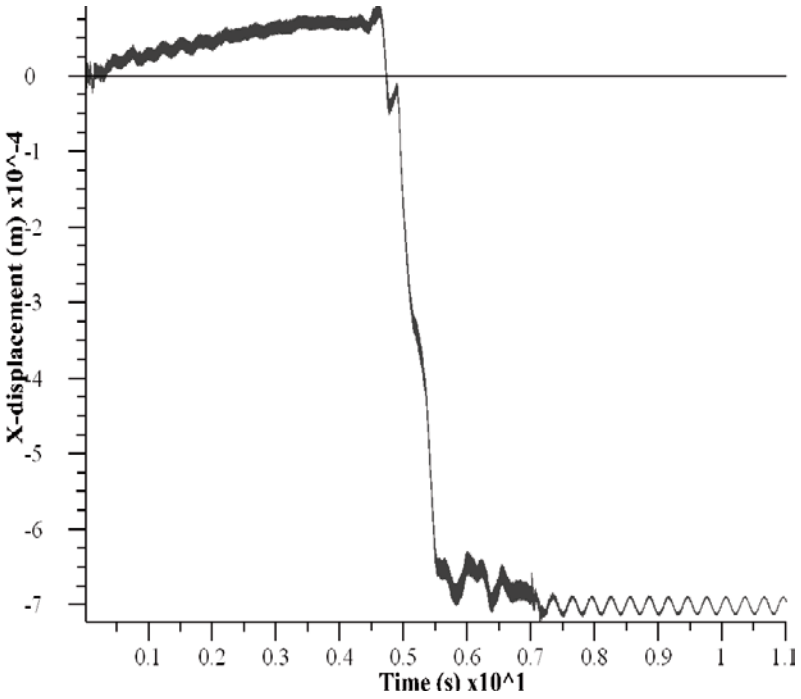

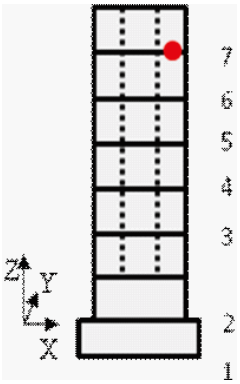

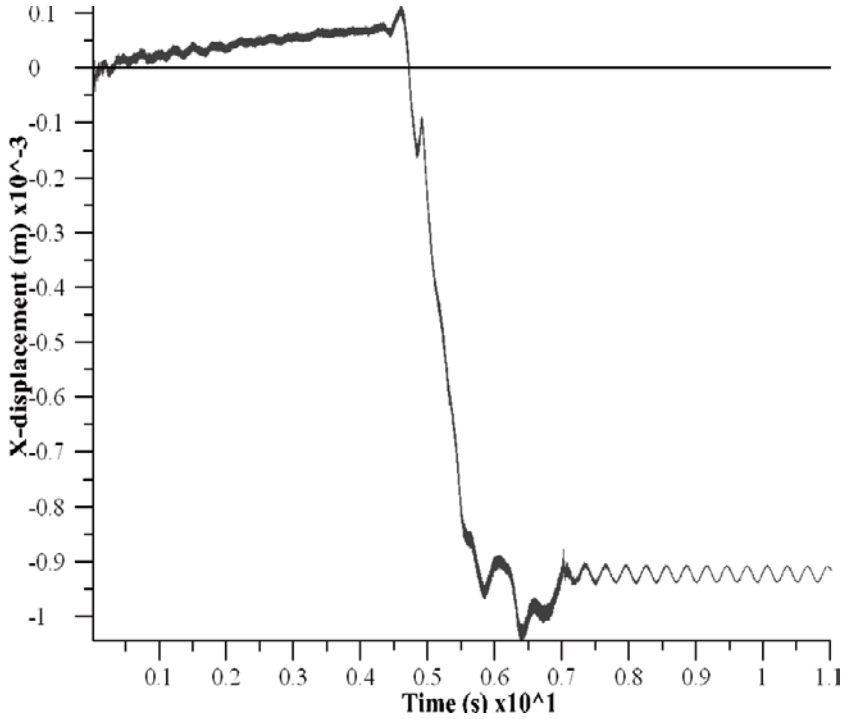

Appendix 6

The natural frequency

History point

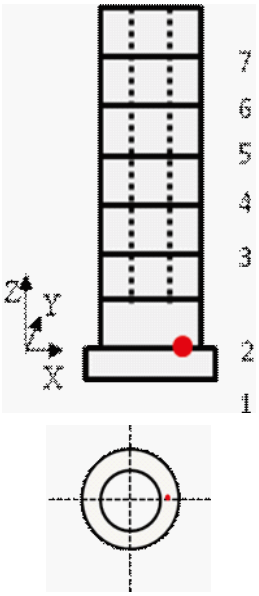

X-Displacement (m) Vs Time (s)

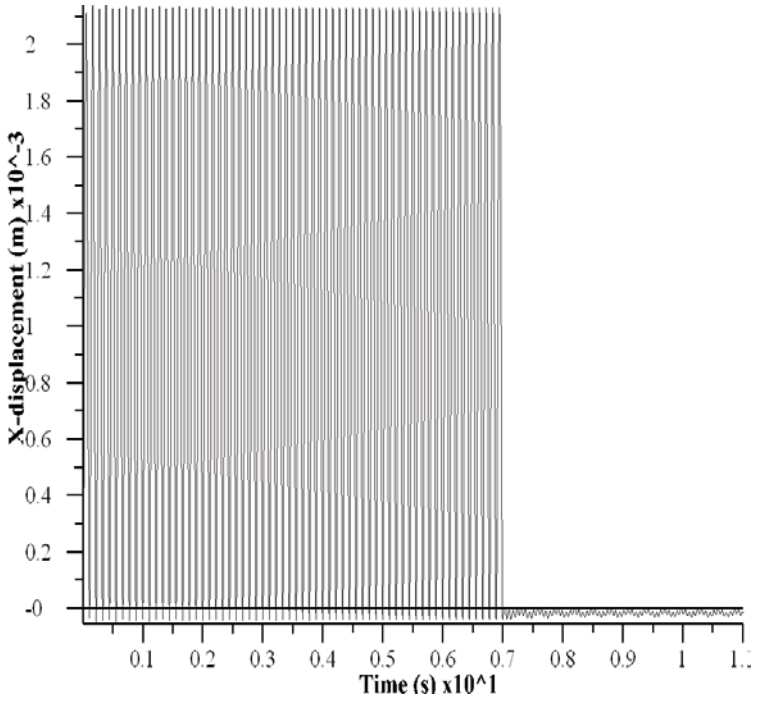

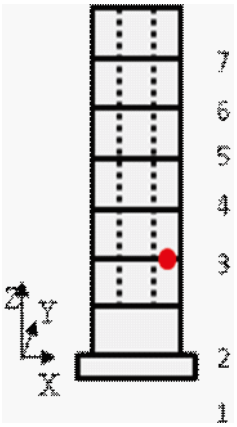

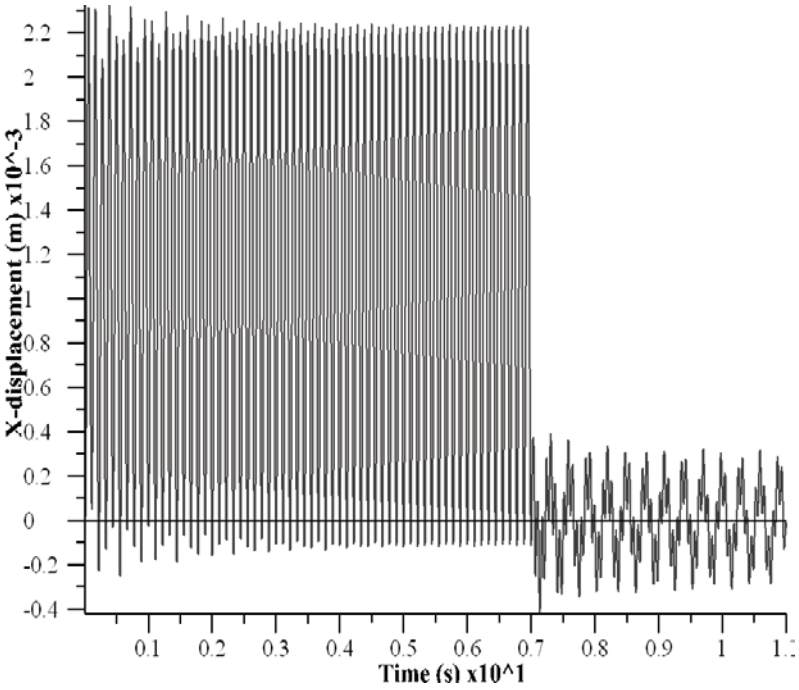

History point

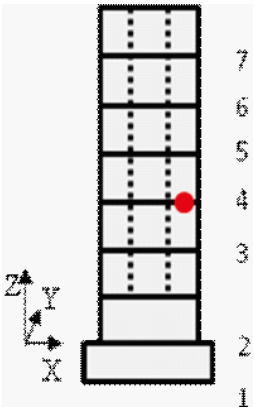

X-Displacement (m) Vs Time (s)

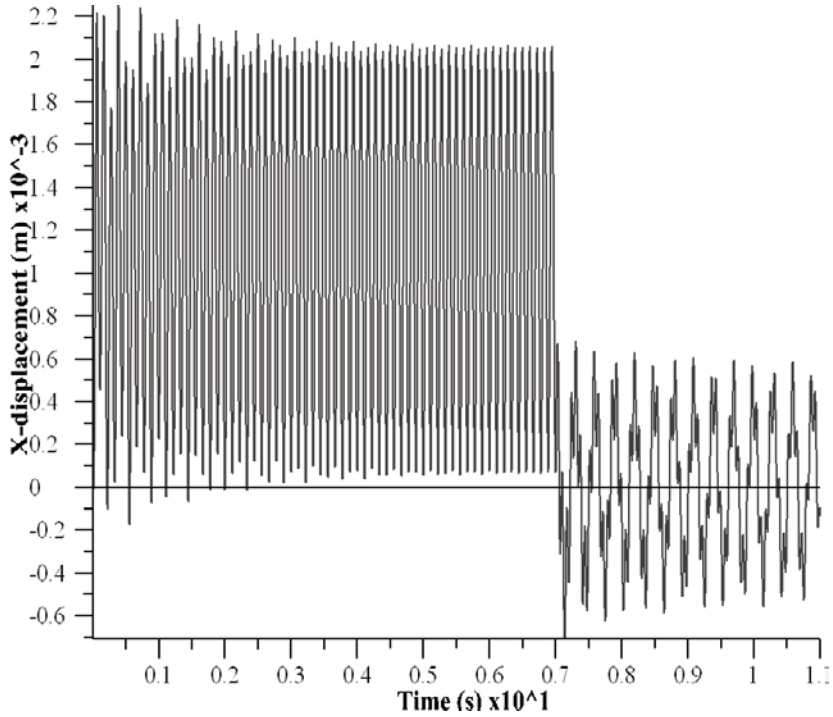

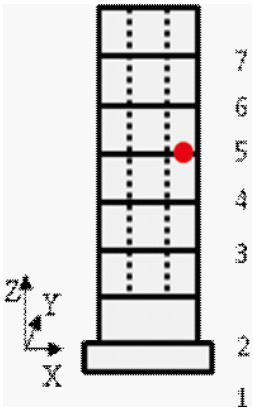

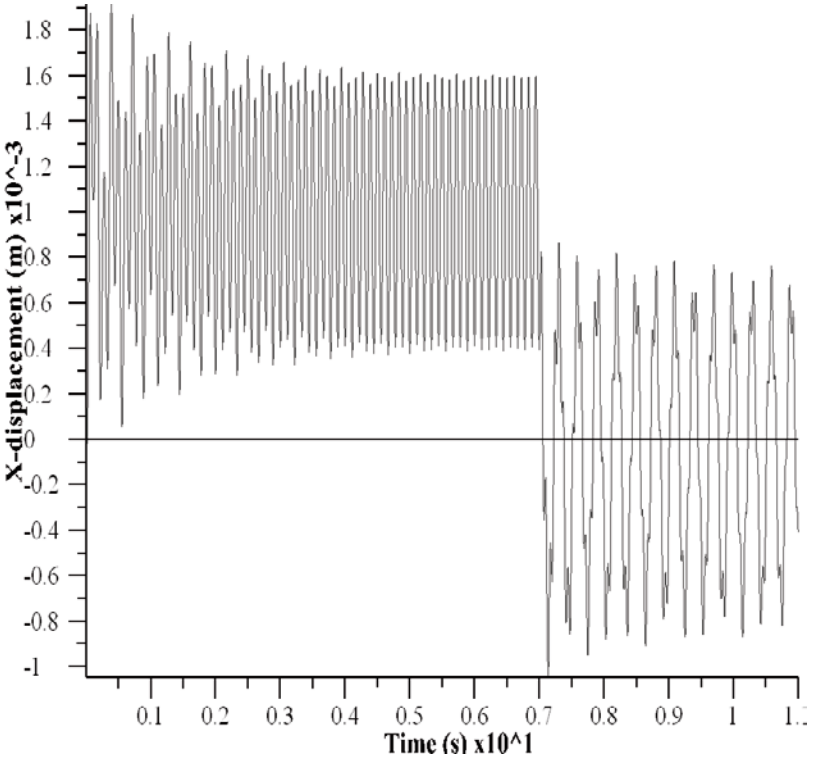

History point

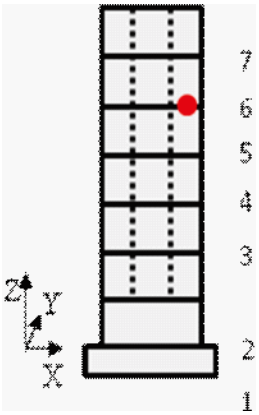

X-Displacement (m) Vs Time (s)

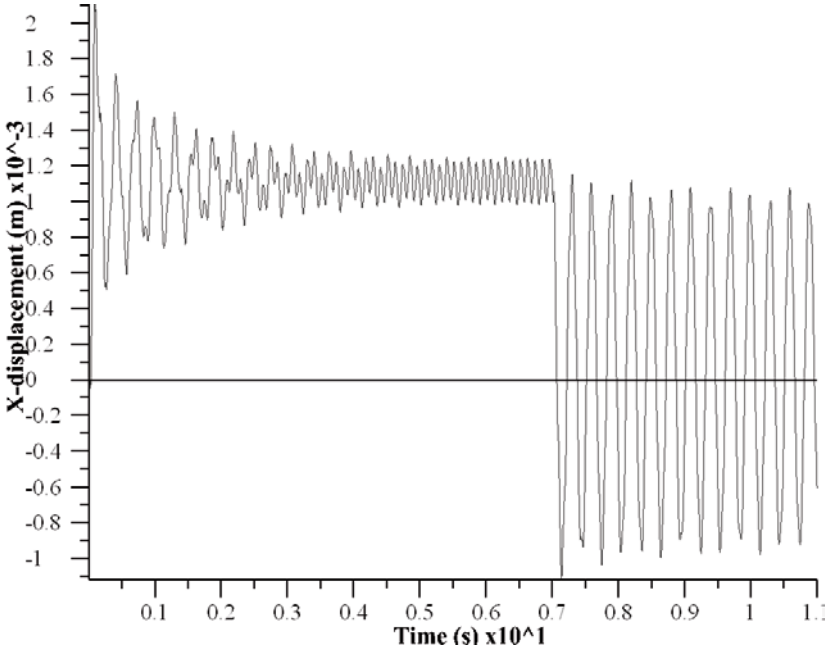

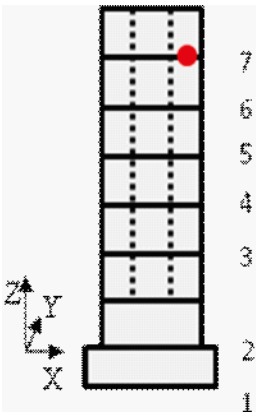

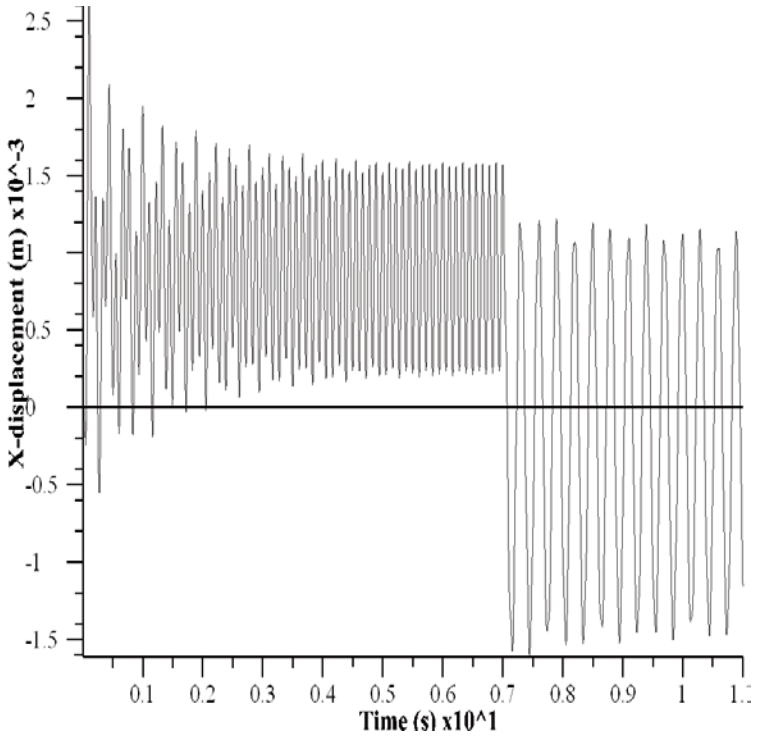

Appendix 7

Sampled blasting wave applied to the bentonite rings

History point

X-Displacement (m) Vs Time (s)

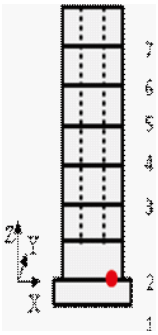

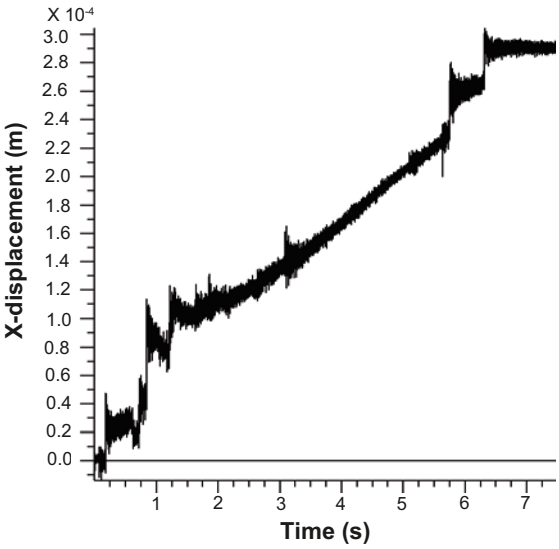

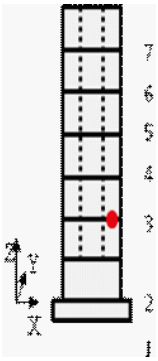

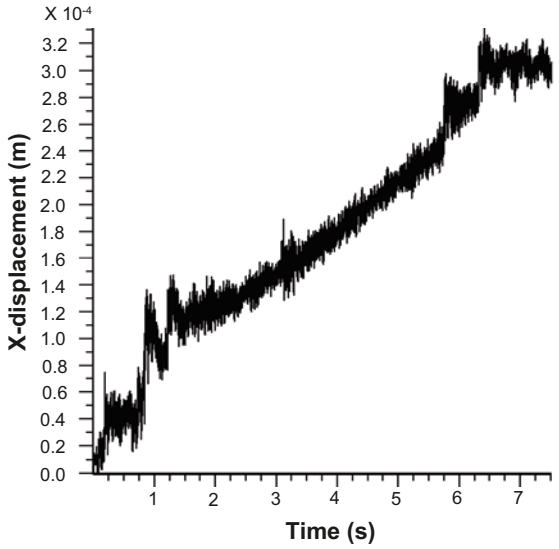

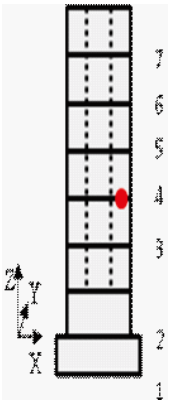

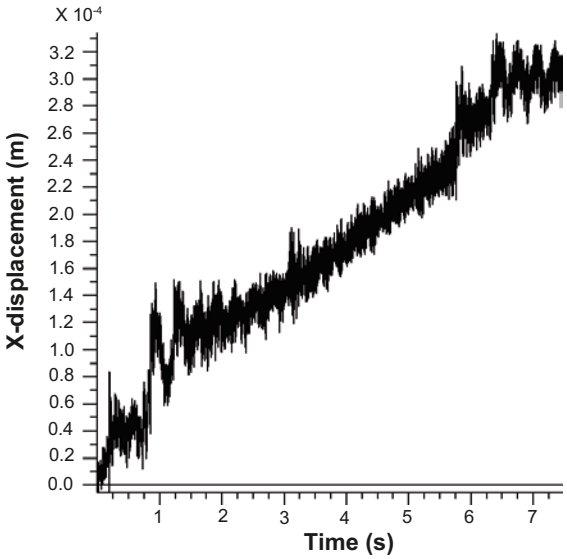

History point

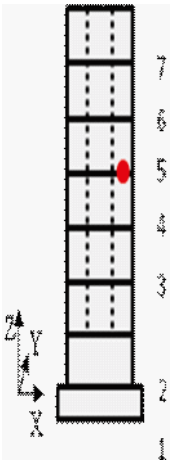

X-Displacement (m) Vs Time (s)